



National Library
of Canada

Bibliothèque nationale
du Canada

Canadian Theses Service

Service des thèses canadiennes

Ottawa, Canada
K1A 0N4

NOTICE

The quality of this microform is heavily dependent upon the quality of the original thesis submitted for microfilming. Every effort has been made to ensure the highest quality of reproduction possible.

If pages are missing, contact the university which granted the degree.

Some pages may have indistinct print especially if the original pages were typed with a poor typewriter ribbon or if the university sent us an inferior photocopy.

Reproduction in full or in part of this microform is governed by the Canadian Copyright Act, R.S.C. 1970, c. C-30, and subsequent amendments.

AVIS

La qualité de cette microforme dépend grandement de la qualité de la thèse soumise au microfilmage. Nous avons tout fait pour assurer une qualité supérieure de reproduction.

S'il manque des pages, veuillez communiquer avec l'université qui a conféré le grade.

La qualité d'impression de certaines pages peut laisser à désirer, surtout si les pages originales ont été dactylographiées à l'aide d'un ruban usé ou si l'université nous a fait parvenir une photocopie de qualité inférieure.

La reproduction, même partielle, de cette microforme est soumise à la Loi canadienne sur le droit d'auteur, SRC 1970, c. C-30, et ses amendements subséquents.

THE UNIVERSITY OF ALBERTA

**An Experimental Verification of
a Treatment Planning Algorithm for
Photon Dose Calculations in Irregular Fields**

BY

TREVOR M. FITZGERALD

A THESIS

SUBMITTED TO THE FACULTY OF GRADUATE STUDIES AND RESEARCH IN

PARTIAL FULFILMENT OF THE REQUIREMENTS FOR THE DEGREE OF

MASTER OF SCIENCE

IN

MEDICAL PHYSICS

DEPARTMENT OF PHYSICS

EDMONTON, ALBERTA

SPRING, 1989



National Library
of Canada

Bibliothèque nationale
du Canada

Canadian Theses Service Service des thèses canadiennes

Ottawa, Canada
K1A 0N4

The author has granted an irrevocable non-exclusive licence allowing the National Library of Canada to reproduce, loan, distribute or sell copies of his/her thesis by any means and in any form or format, making this thesis available to interested persons.

The author retains ownership of the copyright in his/her thesis. Neither the thesis nor substantial extracts from it may be printed or otherwise reproduced without his/her permission.

L'auteur a accordé une licence irrévocable et non exclusive permettant à la Bibliothèque nationale du Canada de reproduire, prêter, distribuer ou vendre des copies de sa thèse de quelque manière et sous quelque forme que ce soit pour mettre des exemplaires de cette thèse à la disposition des personnes intéressées.

L'auteur conserve la propriété du droit d'auteur qui protège sa thèse. Ni la thèse ni des extraits substantiels de celle-ci ne doivent être imprimés ou autrement reproduits sans son autorisation.

ISBN 0-315-52812-5

THE UNIVERSITY OF ALBERTA
RELEASE FORM

Name of Author: TREVOR M. FITZGERALD

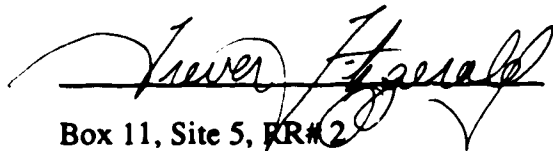
Title of Thesis: **An Experimental Verification of a Treatment
Planing Algorithm for Photon Dose
Calculations in Irregular Fields.**

Degree: Master of Science

Year this Degree Granted: 1989

Permission is hereby granted to the UNIVERSITY OF ALBERTA LIBRARY to reproduce single copies of this thesis and to lend or sell such copies for private, scholarly, or scientific research purposes only.

The author reserves other publication rights, and neither the thesis nor extensive extracts from it may be printed or otherwise reproduced without the authors written permission.



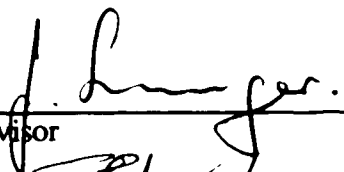
Box 11, Site 5, RR#2

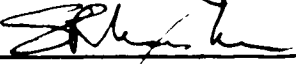
Winterburn, Alberta, T0E 2N0

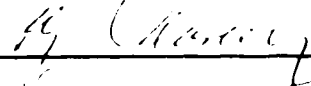
Date: May 13/1989

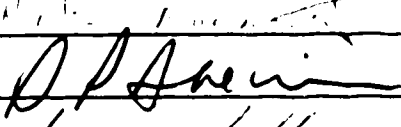
THE UNIVERSITY OF ALBERTA
FACULTY OF GRADUATE STUDIES AND RESEARCH

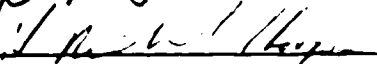
The undersigned certify that they have read, and recomend to the Faculty of Graduate Studies and Research for acceptance, a thesis entitled, **An Experimental Verification of a Treatment Plannig Algorithm for Photon Dose Calculations in Irregular Fields**, submitted by **Trevor M. Fitzgerald** in partial fulfilment of the requirements for the degree of **Master of Science in Medical Physics**.



Supervisor








Date: _____

**This work is dedicated to my parents,
Chuck and Esther,
who gave to me greatly appreciated support**

ABSTRACT

Shielding blocks are commonly used to protect critical physiological structures, during radiation therapy with megavoltage photon beams. The computer program "Irreg" [3], which models the scattered radiation, is a useful treatment planning tool for predicting the dose at points of interest within these irregular fields.

An experimental verification of Irreg+, an improved version of the Irreg algorithm, developed at the Cross Cancer Institute, was undertaken. Measurements with ionization chamber and small diode dosimeters demonstrated Irreg+ modeled the scatter well in most conditions. A few problem areas arose, with the worst discrepancies occurring in the Co-60 calculations. The errors could be traced to the parameterization of the extended source model, which calculates the scatter off the collimator in the program. A discussion of the performance of Irreg+ will be given for calculations with Co-60, 6MV, and 15MV X-rays, and a verification of the extended source model will be presented.

ACKNOWLEDGMENTS

I would like to express my sincere thanks and appreciation to the following people who assisted me in making this thesis possible.

My girlfriend, Jody Tetreau, for her patience and tolerance of being stood up for an accelerator on many occasions.

My supervisors, Dr. John Scrimger and Dr. J.J. Battista for their enthusiasm, guidance, technical assistance, and editorial help.

John Isitt, and the mould room staff, as well as Finn Mortenson and the machine shop staff for fabricating materials necessary for this research.

The Radiation Oncology Department for the use of their computer network, and printer.

Collin Field, John Antolak, and Ernest Mah for their computing help and technical assistance.

Fellow students Don Robinson and Atsushi Takahashi for listening, and trading ideas

The Physics Department of the University of Alberta for their financial support,

and to all others who assisted me with this work.

TABLE OF CONTENTS

	Page
List of Tables	ix
List of Figures	xi
1 INTRODUCTION	1
1.1 Introduction	2
1.2 Radiotherapy Treatment Planning	2
1.3 Irregular Fields	4
1.5 Treatment Modalities	6
1.5 Radiation Interactions	8
1.6 Dose Deposition	12
1.61 Dose Build up and Depth Dose	13
1.7 Dose measurement	16
2 DOSE CALCULATION METHOD WITHIN IRREGULAR FIELDS	19
2.0 Introduction	
2.1 The Irreg+ Algorithm	19
2.11 Tissue-Air Ratios and Scatter-Air Ratios	19
2.12 Sector Integration of Scatter	25
2.13 Sector Integration of Primary, the Extended Source Model	27
2.2 Problems with the Irreg+ Algorithm, and need for Experimental Verification	30
3 METHOD AND MATERIALS	31
3.1 Irradiation Conditions	32
3.2 Measurements	37
3.3 Accuracy of the Measurements	38
3.4 The Diode Response versus the Ion Chamber	41
3.41 Introduction	41
3.42 Angular Dependent Response Variations	41

	3.43	Energy Dependent Response Variations	45
	3.44	Conclusions on the Acceptability of the Diode Measurements	47
4		RESULTS AND INTERPRETATION	48
	4.0	Results and interpretation of data	49
	4.1	Results	49
	4.2	Discussion of the Results	60
	4.21	Trends in the Co-60 Data	61
	4.22	Trends in the 6 MV Data	62
	4.23	Trends in the 15 MV Data	63
	4.3	Clinical Significance of the Discrepancies	64
	4.4	Sources of Error in the Irreg+ Algorithm	68
	4.5	Verification of the Extended Source Parameter, α	72
	4.6	Discussion of the Results of the Modified Irreg+ Calculations	79
	4.61	Modified Irreg+ Results for Co-60	79
	4.62	Modified Irreg+ Results for 6 MV	80
	4.63	Modified Irreg+ Results for 15 MV	81
5		CONCLUSIONS	83
	5.0	Summary and Conclusions	84
	5.1	Future Work	85
6		REFERENCES	88
	6.0	References	89

LIST OF TABLES

<u>Table</u>	<u>description</u>	<u>page</u>
3-1	Summary of rectangular shielding block thicknesses	35
3-2	Summary of square shielding block thicknesses	36
3-3	Summary of shielding block dimensions and their projected shadow sizes	37
4-1	Measured and calculated effective transmissions in Co-60 under 2 x 7 cm ² spinal shields	51
4-2	Measured and calculated effective transmissions in Co-60 under 1 x 7 cm ² spinal shields	52
4-3	Measured and calculated effective transmissions in Co-60 under square occlusion blocks	53
4-4	Measured and calculated effective transmissions in 6 MV under 2 x 7 cm ² spinal shields	54
4-5	Measured and calculated effective transmissions in 6 MV under 1 x 7 cm ² spinal shields	55
4-6	Measured and calculated effective transmissions in 6 MV under square occlusion blocks	56
4-7	Measured and calculated effective transmissions in 15 MV under 2 x 7 cm ² spinal shields	57
4-8	Measured and calculated effective transmissions in 15 MV under 1 x 7 cm ² spinal shields	58
4-9	Measured and calculated effective transmissions in 15 MV under square occlusion blocks	59

4-10	Frequency of significant discrepancies	67
4-11	Nominal narrow beam transmissions and their measured estimates for each block	71
4-12	Summary of rms errors in Co-60 data	79
4-13	Summary of rms errors in 6 MV data	81
4-14	Summary of rms errors in 15 MV data	81

LIST OF FIGURES

<u>Figure</u>	<u>description</u>	<u>page</u>
1-1	Clinical example of an irregular field and spinal shielding block usage	5
1-2	Cobalt -60 isotope capsule	7
1-3	Variation with energy of the mass attenuation coefficients of the basic interactions with energy	11
1-4	Depth dose curve for 6 MV radiation	15
2-1	Scatter and primary components of dose	21
2-2	SAR/TAR plotted versus depth for Co-60	23
2-3	SAR/TAR plotted versus field radius for Co-60	24
2-4	Arbitrary field shape divided into circular sectors	26
2-5	The extended source model	28
3-1	Experimental set up	33
3-2	The Capintec ion chamber	34
3-3	Blocked and open field dose profiles	40
3-4	The diode	42
3-5	Response of the diode versus incident angle of radiation	43
3-6	Response of the diode and ion chamber versus energy	46
4-1	Rings of iso-intensity of the extended source seen by a dose point at the field edge	74
4-2	Strip of the extended source function through its center	75

4-3	Measured dose gradient, $d/dy[dD/dx]$, versus distance from field corner	76
4-4	Log of the dose gradient versus corner distance	77
5-1	Measured and calculated transmissions versus depth	86

CHAPTER 1

INTRODUCTION

1.1 Introduction

Since Roentgen first discovered X-rays in 1895, many researchers have studied their properties, and some of them discovered the harmful effects of radiation through first hand experience. While this was unfortunate for them, it did lead to the development of many of the medically beneficial uses of radiation, and in particular, radiotherapy for cancer. Grubbe and Despeignes [1] applied radium to inoperable carcinomas in 1896, which was the first documented treatment of cancer with radiation. Today in Alberta, about 55% of cancer patients have the disease treated partially, or completely with radiation.

There are two primary modes of radiation delivery to a diseased region: brachytherapy and teletherapy. Brachytherapy involves placement of radioactive sources within the body, usually inside the tumor volume. Teletherapy, as the name implies, is treatment using a radiation beam which originates some distance outside the body. This thesis will deal with aspects of dose calculations for external X-ray beams.

1.2 Treatment Planning

Complications arise in radiotherapy when healthy tissue near the tumor receives a higher dose than it can tolerate, or when the tumor dose is insufficient for control. The effects of both these competing processes are minimized by good radiotherapy treatment planning.

Radiotherapy treatment planning is the discipline which involves selecting the appropriate beam energy, number, shape, angle of approach and shielding in order to achieve the most favorable dose distribution. This process can be iterative and relies heavily on accurate dose calculations and measurements, provided by the medical physicist. For acceptable treatment, the dose received by the target volume should be within 5% of the prescribed value [2]. Since errors arise from an inability to duplicate the exact patient position for each fraction of the treatment, an accuracy of 2-3% in the dose computations is desirable.

Since the early 1970's, computers have been used to calculate dose distributions. One of the early dose calculating programs, Irreg, was developed by J. Cunningham [3], based on Clarkson's method [4]. The algorithm is still widely used today. The calculations performed by Irreg are based on empirical 'look-up' tables which give the attenuated primary and scatter components of the dose for various depths and field sizes. The strengths of this program are that it can easily deal with irregularly shaped fields, (hence the name), and it uses very little computer time to do a calculation.

Many modern computerized treatment planning systems use modified versions of the original Irreg algorithm. At the Cross Cancer Institute, a version called Irreg+ is used. The major difference between the two is that Irreg+ can account for partial transmission of a beam through shielding blocks, whereas Irreg cannot, and assumes no transmission through blocks in the field. Other dose calculation techniques which are more accurate than Irreg+, and are based on the Monte Carlo method, have

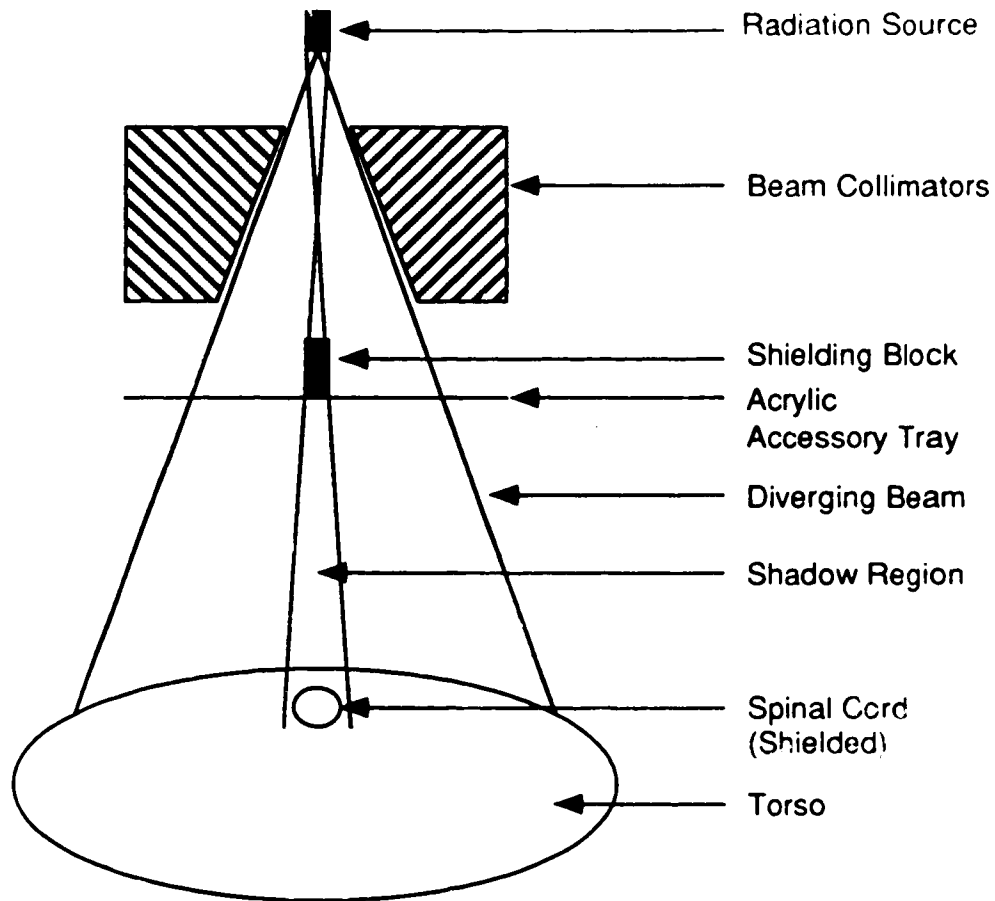
been or are being developed. However, their difficulty of implementation and lengthy computational times makes them clinically impractical at this time. Although Irreg+ is practical, it has difficulties in predicting the dose under narrow shielding blocks placed in the treatment field. In fact, many commercial treatment planning systems have difficulty predicting the dose under small blocks, as was reported by Tatcher [5]. This thesis will investigate the conditions where the Irreg+ dose calculations are inaccurate, and suggest solutions to the problems.

1.3 Irregular Fields

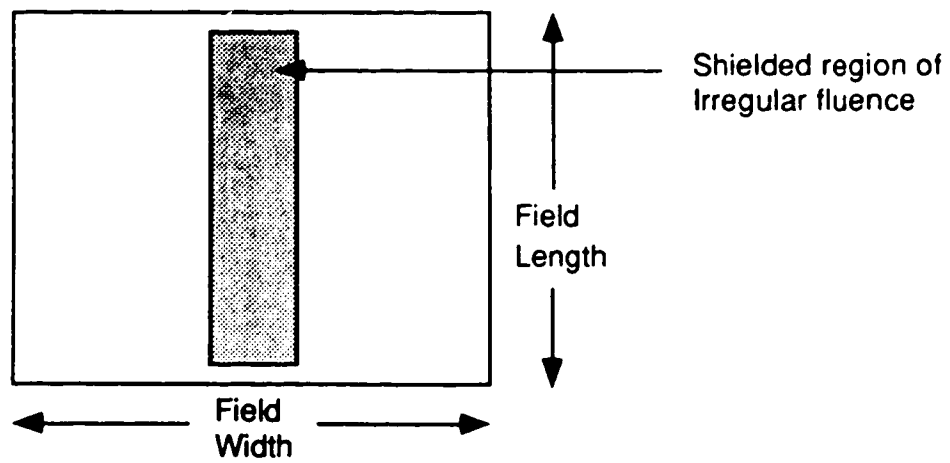
It is a common radiotherapy technique to place beam occluding blocks in a treatment field, in order to shield sensitive physiological structures, or to shape the beam. The blocks used may be formed from lead, cerrobend, or other high density materials. Fields which employ blocks and have a non-uniform fluence, or non-rectangular shape are known as irregular fields. As the name implies, the Irreg+ algorithm is designed to deal with dose calculations in irregular fields.

An example of shielding block use, and an irregular field is shown in figure 1-1, where a long narrow block has been used to shield the spinal cord, which is a sensitive structure. When situations such as these occur, the radiation oncologist requires accurate dose distribution information from the treatment planners to ensure that the sensitive structure is shielded sufficiently, and also that the whole tumor volume is treated adequately.

figure 1-1 Lateral View
of a shielding
block usage



Beams eye view



1.4 Treatment Modalities

There are two principal types of external beam radiation employed in radiotherapy. These are beams consisting of either high energy photons, or electrons. The source of both these beams is usually a medical linear accelerator (linac), and in the case of photons, high activity isotopes can also be used. Most of the isotope machines in use today employ Co-60, (half life = 5.26 years), which is produced by neutron activation of Co-59. The useful radiation from Co-60 are two gamma rays, 1.17 and 1.33 MeV, emitted in cascade when it decays to Ni-60. For ease of handling, standard cobalt source capsules have been developed, their construction is shown in figure 1-2. The sources consist of an outer and an inner stainless steel cylinder in which many tiny radioactive cobalt pellets are sealed. Their diameter is around 1.75 cm, with a height about the same. The capsules have an activity near 10 TBq/g when new, which produces a photon fluence on the order of $10^9 \text{ cm}^{-2} \text{ s}^{-1}$, at a distance of 80 cm from the source. This translates to an absorbed dose in air near 200 cGy/min.

Medical linear accelerators are available with energies ranging from 4 to 35 MeV, and many can produce both electron and photon beams. When operating in photon mode, a tungsten target is inserted into the electron beam, which produces a thick target bremsstrahlung spectrum of X-rays. The mean photon energy is between 1/3 and 1/2 of the electron beam energy. Past the target a specially shaped tungsten filter is inserted in the beam which preferentially absorbs the radiation so that the X-ray fluence will

Figure 1-2, Photograph showing the inner and outer containers, and radioactive pellets of a Cobalt-60 source. Taken from Cunningham and Johns 'The Physics of Radiology' [6].



be uniform over a large field. This device is known as a beam flattening filter. Usually thin filters of copper or aluminum are also placed in the beam to absorb the low energy photons which are harmful to the surface layers of the patient but have little effect on a deep tumor.

Radiation from the sources described above is generally measured with one of four methods that can handle the high dose rates which occur. These four methods are, ionization chambers, diodes, thermoluminescent dosimetry, and film. Ion chambers and diodes respond very linearly with the amount of radiation received, whereas film has a limited linear response region. Film, however is sensitive to small changes in exposure over a large area, so diagnostic images can be produced. Thermoluminescent dosimetry, or TLD, makes use of thalium doped lithium flouride, or other suitable powders. When electrons are excited during irradiation, impurity induced crystal imperfections 'trap' a fraction of them in a normally disallowed energy band. When the sample is heated, these electrons gain enough energy to 'escape' and then return to an allowed lower energy level, emitting visible light in the process. The amount of light emitted from a sample is proportional to the dose received. The small size of the TLD samples makes them a useful tool for checking the surface dose of patients treated with irregular fields.

1.5 Radiation Interactions

The next two sections will deal with the basic photon interactions with matter and concepts of dose deposition. As well, some important terms and

units used in this text will be defined. Primary and secondary energy transfer reactions will be discussed and related to dose deposition.

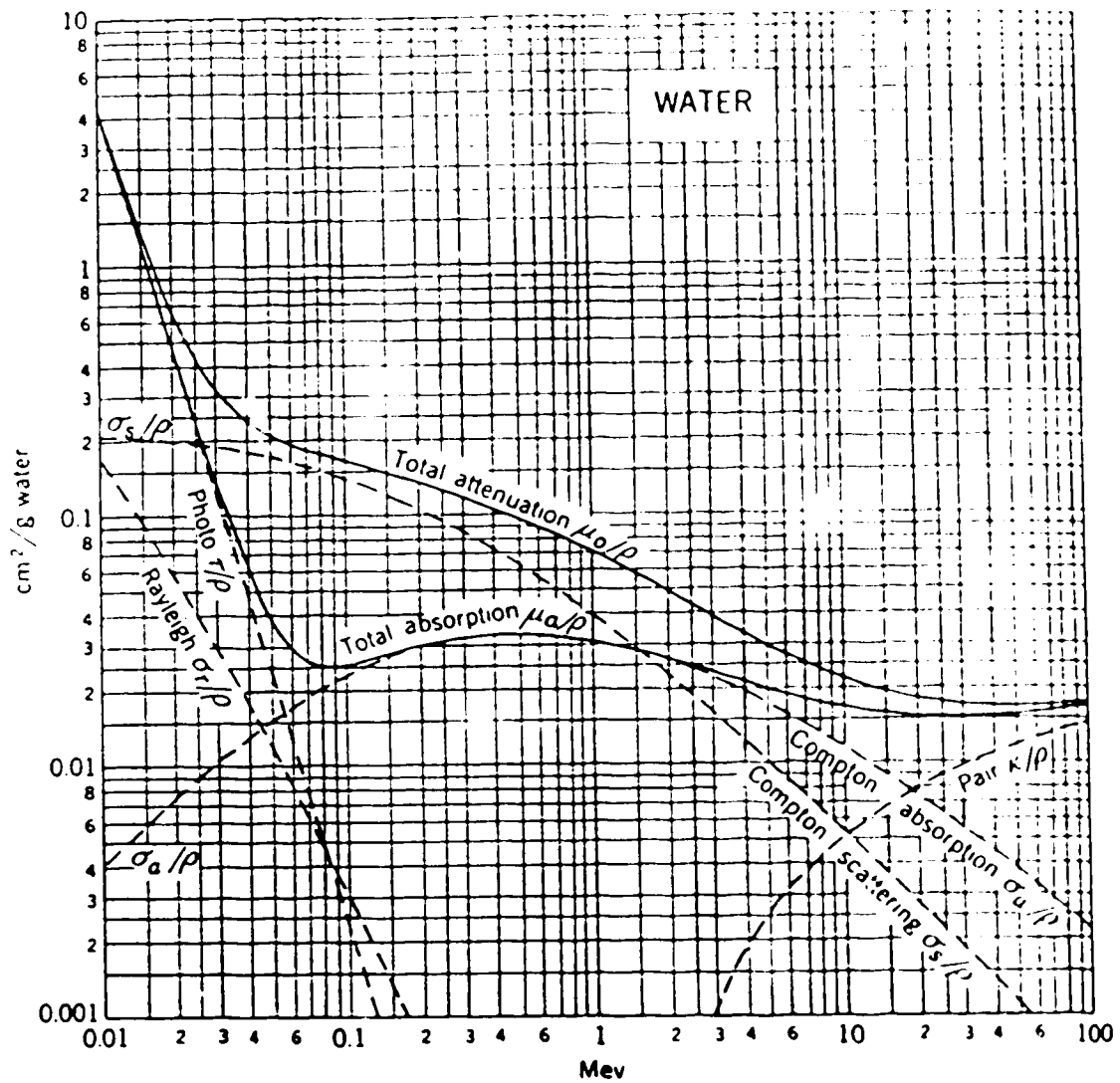
In the photon energy range of interest there are three basic interactions which occur. These are; the photoelectric effect, Compton scattering, and pair production. The photoelectric effect occurs when a photon collides with an atom, and transfers all its energy to a single electron, thus ejecting it from its orbit. Compton scattering involves only a fractional transfer of energy from a photon to an electron in a collision. The electron is ejected from the atom, and the photon is deflected in the process. Pair production is the result of a photon interacting in the field of an electron or nucleus, and initiating the creation of an electron-positron pair from its energy. The threshold energy for pair production is the combined rest mass energy of the particle pair, 1.022 MeV, with any excess appearing as kinetic energy distributed between the two particles.

The occurrence probability for these three radiation processes depends on the energy of the incident radiation beam and on the atomic number and density of the absorber. For water, which emulates soft tissue, the photoelectric effect is negligible for energies above 60 KeV, where its interaction cross section is about one tenth that of the Compton cross section. This is because the photon energy has become much greater than the binding energy of the electrons and the probability of a photoelectric event decreases with this energy difference. Compton scattering events which occur more readily with the outer loosely bound electrons are dominant up to about 5 MeV, where pair production has a contribution of about 10% to the total cross section. At 25 MeV, pair production overtakes Compton

scattering as the leading contributor to the total interaction cross section. The above can be observed in figure 1-3, which shows the variation with energy of the mass attenuation coefficients of water, for each processes. Mass attenuation coefficients are linear attenuation coefficients divided by the density of the absorbing material, so that it has units of cm^2/g . The photoelectric coefficient τ/ρ is very large at first, but falls off rapidly with energy. The total compton coefficient, σ_{tot}/ρ , appears in two parts, the mass absorption coefficient, σ_a/ρ and the mass scattering coefficient, σ_s/ρ , which add up to the total. The quantity $\sigma_a/\sigma_{\text{tot}}$ represents the average fraction of the energy of the photon which will be absorbed in a compton event, and $\sigma_s/\sigma_{\text{tot}}$ represents the fraction which will be carried away by the photon. The pair production coefficient, κ/ρ appears on the plot near 3 Mev, and then it increases in a logarithmic manner with energy until it becomes the dominant contributor to the total attenuation coefficient.

On the left side of figure 1-3 is a line for the mass attenuation coefficient for Rayleigh scattering, σ_r/ρ . This process which has not been mentioned previously occurs when the electrons of an atom act as a coherent reflector of a photon. The photon is scattered, with a negligible energy loss to the atom. The process is of little interest, as it has a small interaction probability compared to the other interactions, and it does not contribute to the dose deposited by a beam. A good summary of all the primary photon interactions can be found in Cunningham & Johns [5], and a more detailed discussion with tabulation of the cross sections of many materials for a wide range of energies was produced by Hubbell [7].

figure 1-3. Plot of the mass attenuation coefficients of the photoelectric effect, compton scattering and pair production processes, in water, showing their relative importance over the photon energy range from 0.01 to 100 Mev, reproduced from Evans, [8].



1.6 Dose Deposition

The net result of the interactions mentioned in the previous section, is that charged particles, primarily electrons, and also positrons, are set in motion. These are the minions of dose. Through secondary collisions they are responsible for most of the ionizations which occur throughout the absorbing medium, and ultimately they convert the absorbed radiation into heat, and chemical potential energy. How much dose, or energy, an electron deposits along its track is determined by the ionizational stopping power of the medium. This is the rate at which energy is lost per unit track length, and for an electron is given by the following equation;

$$S_{\text{ion}} = \frac{1}{\rho} \left(\frac{dE}{dX} \right) = 2\pi r_0^2 N_e \frac{\mu_0}{\beta^2} \left[\ln \frac{E^2(E + 2\mu_0)}{2\mu_0 I^2} + \frac{E^2/8 - (2E + \mu_0)\mu_0 \ln 2}{(E + \mu_0)^2} + 1 - \beta^2 - \delta \right]$$

eqn. 1-1

in units of MeV/cm. ρ is the density of the medium, r_0 is the classical electron radius, N_e is the number of electrons per gram, I is the mean excitation energy of the absorber, μ_0 is the electron rest mass energy, β is v/c , and δ is a small density correction factor. For most materials, the stopping power decreases with energy until a minimum of 1-2 MeV/cm is reached near 1 MeV, then it slowly increases with energy. The range of an electron is the integral of the stopping power over the energy, but due to scattering the actual penetration depth is reduced. In water, electrons with an initial energy between 1 and 20 MeV have a penetration depth in cm which is approximately half their initial energy in MeV [9].

The amount of energy transferred from a photon fluence to an absorbing medium's electrons is described by the Kinetic Energy Released per unit Mass, or KERMA. If one considers a thin layer of absorber at a depth d , then the KERMA at d is all the energy which is transferred to the electrons in that layer. KERMA, like the photon fluence, is a maximum at the surface and then decreases exponentially with depth as interactions remove photons from the beam. The Absorbed Dose is that part of the transferred energy which is locally retained in the medium. It does not include energy carried out of the region by fast electrons, or bremsstrahlung. The units of absorbed dose, and KERMA, are the Joule/Kg, or Gray (Gy).

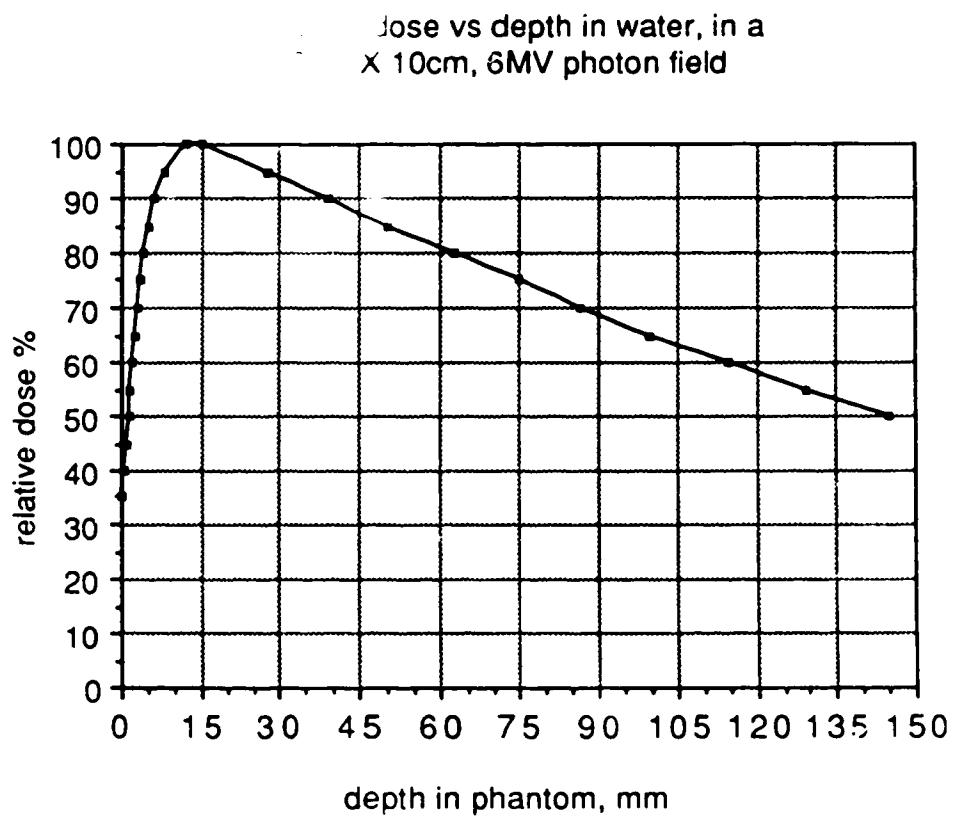
1.61 Dose Build up, and Depth Dose

Now that energy transfer has been discussed, it should be mentioned how the dose changes with depth in an absorber in a large radiation field. With the photon energies used in radiotherapy, the electrons set in motion near the surface have a range up to a few centimeters. The KERMA is much greater than the absorbed dose near the surface, because the electrons have carried the energy deeper into the medium. This situation is known as electronic disequilibrium, because if a thin layer is considered, more electrons are leaving the layer than are entering it. As the depth increases, the number of electrons entering a layer increases, and the absorbed dose approaches the KERMA, this is known as the build up region. At a certain depth the number of electrons entering and exiting a layer will balance, creating electronic equilibrium, and the absorbed dose will equal the KERMA. This point is also where the maximum dose is deposited, and is called D_{max} , or the maximum dose depth. Beyond this depth, the dose

decreases as the KERMA decreases, and electronic disequilibrium occurs again, as more electrons are entering a layer from above, than are exiting it. However, this disequilibrium is small enough to be ignored for most practical purposes, and the region is referred to as having pseudo equilibrium.

The above phenomena are demonstrated in figure 1-4, a depth dose curve in water at the center of a $10 \times 10 \text{ cm}^2$ field, irradiated with 6 MV X-rays, using a 100 cm source to surface distance (SSD). The depth where the maximum dose occurs, D_{max} , is approximately 1.5 cm. The build up region is seen before D_{max} , and after it is the region of pseudo electronic equilibrium, where the dose falls off slowly as the photon beam is attenuated. The characteristics of a depth dose curve are dependent on field size, beam energy, and the SSD.

Figure 1-4 Measured depth dose curve for 6 MV radiation.



1.7 Dose Measurement

Ionization chambers are predominantly used to measure absorbed dose in phantoms. These chambers contain a known mass of air, which has a known mean ionization potential, W , of 33.85 eV per ion pair created. When irradiated, the ions produced are collected and an electrometer allows the current to be determined. If the current is integrated, the total charge liberated, Q , can also be determined. This number multiplied by the ionization potential gives the total energy absorbed by the air, which gives the dose when divided by the mass. In practice, certain conditions must be adhered to, and a number of correction factors must be applied to the instrument reading in order to obtain an absorbed dose measurement.

Ionization chamber measurements are based on Bragg-Gray cavity theory, which is discussed in Johns [5]. A brief summary of the principles involved will be stated here. The ion chamber cavity must be surrounded by enough phantom medium so that electronic equilibrium occurs, and a uniform fluence of electrons is present in the cavity. The wall of the chamber must be of a material with similar radiologic properties as the medium, so that it does not greatly perturb the electron fluence entering from the medium. Essentially, the air in the cavity sees the same electron fluence as the wall, (if the previous two conditions are met), therefore the ratio of the wall dose to the air dose is a ratio of their averaged stopping powers, $\bar{S}_{\text{air}}^{\text{wall}}$. The term averaged is used because the stopping powers are averaged over the electron energy spectrum, which in turn is generated by averaging over the photon spectrum of the beam. The net result of all this is that the

absorbed dose to the cavity wall can be related to the ionization of the air by the Bragg-Gray formula;

$$D_{\text{wall}} = \frac{Q}{m_{\text{air}}} W \bar{S}_{\text{air}}^{\text{wall}} \quad \text{eqn. 1-2}$$

Similarly, the dose to the medium can be obtained by multiplication with a ratio of the KERMA's of the medium and the wall, assuming electronic equilibrium exists in the medium. Strict protocols for obtaining absorbed dose measurements in a phantom, as well as all the correction factors which must be applied are discussed in the ICRU REPORT #23 [10]

CHAPTER 2

DOSE CALCULATION METHOD

WITHIN IRREGULAR FIELDS

2.0 Introduction

The difficulties of predicting the dose in irregular fields were recognized many years ago, and to deal with these cases, Clarkson, in 1941 [4] developed a calculational method that was suitable for clinical use. In 1971 this method was incorporated into the computer program Irreg, by J. Cunningham [3]. Clarkson's method relies on the fact that the dose at a point in a field consists of primary and scattered radiation components. These components have been tabulated for many depths and field radii. Thus, any shape of field can be divided into small circular segments for which the fractional scatter component may be summed to give the total scatter. This is then added to the primary component, which is only depth dependent, to obtain a value for the total dose. The next section will expand on the details of this method, and in particular, on how the operations are performed within the Irreg+ dose calculating algorithm.

2.1 The Irreg+ Algorithm

2.11 Tissue-Air Ratios, and Scatter-Air Ratios

This section will define and describe the use of two important quantities of medical radiation dosimetry; tissue-air ratios, or TAR's, and scatter-air ratios, or SAR's. The tissue-air ratio relates the dose at a point in a water equivalent phantom in a radiation field, to the dose that point would receive if it were in air, surrounded only by enough phantom material to give complete electron build up.

Written as an equation the relationship is:

$$\frac{D_{TIS}}{D_{AIR}} = TAR \quad \text{eqn 2-1a}$$

or

$$D_{TIS} = D_{AIR} \times TAR \quad \text{eqn 2-1b}$$

where D_{AIR} is the dose received by the point 'in air', and D_{TIS} is the dose received by the point in the phantom. The TAR can be seen as a ratio of the two doses, or a factor which converts the 'in air' dose to a tissue dose, as shown in figure 2-1. Tissue air ratios are independent of the source to surface distance, SSD, but they are a function of the field size, W, depth, d, and photon energy, hv. If one considers the TAR for a pencil beam or a 'zero area field', $TAR(0,d,hv)$, it is just the primary transmission to a depth, d. As the field size increases, both the dose and the TAR increase due to the increased contribution of scattered radiation reaching the dose point. Following this line of reasoning, one can decompose the TAR at a point into two components, a primary component, $TAR(0,d,hv)$, and a scatter component, known as the scatter-air ratio, or, $SAR(W,d,hv)$. The sum of the two components must equal the total TAR. Expressing this mathematically, we have:

$$TAR(W,d) = TAR(0,d) + SAR(W,d) \quad \text{eqn. 2-2}$$

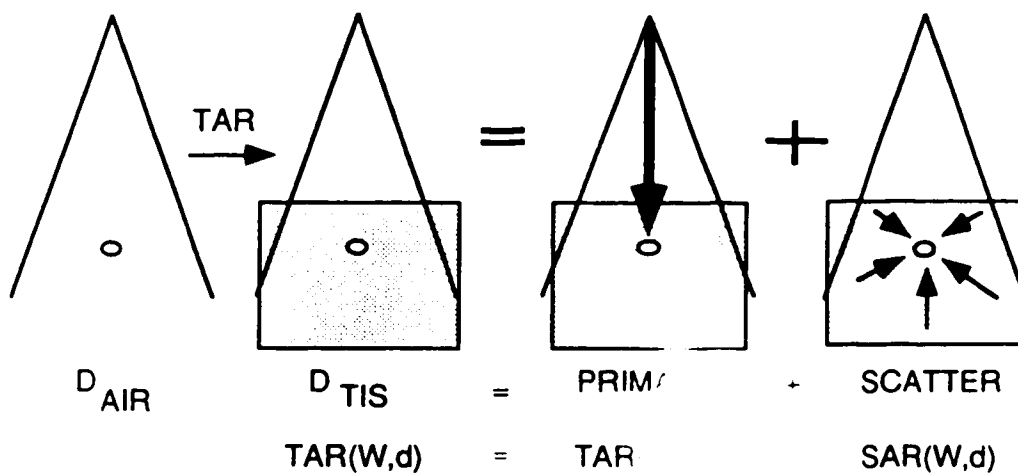
therefore the dose can be written in two components as:

$$D_{TIS} = D_{AIR} \times [TAR(0,d) + SAR(W,d)] \quad \text{eqn. 2-3}$$

this is also shown diagrammatically in figure 2-1, which displays the scatter and primary components of the dose.

figure 2-1 The tissue air ratio at a point is defined as, the dose in air/ the dose in tissue at that point, written as,

$$\frac{D_{TIS}}{D_{AIR}} = TAR \quad \text{or} \quad D_{TIS} = D_{AIR} \times TAR$$



Tissue-air ratios are spectrum dependent, hence they are machine dependent, and must be measured for each radiation unit. They are measured and compiled for a wide range of rectangular field sizes and depths, and then converted to circular field equivalents, written $TAR(r,d)$, where r is the radius of a circular field necessary to produce the same tissue air ratio as the given rectangular field. The zero area field ratios, $TAR(0,d)$, are extrapolated from the data, and circular equivalent scatter air ratios, $SAR(r,d)$, are obtained by subtraction of the $TAR(0,d)$ from the $TAR(r,d)$ values. A demonstrative quantity for the scatter portion of the dose at a point is the quotient, SAR/TAR , which is the fraction of the total dose at a point due the scattered radiation.

In figures 2-2, and 2-3, this quantity is plotted versus depth for a constant field size of $10 \times 10 \text{ cm}^2$, and versus field radius for a constant depth of 4 cm, in Co-60 radiation at 80 cm SSD. It is seen in figure 2-2 how the scatter contribution increases rapidly with depth, as the primary is attenuated, and more scattered photons find their way back to the dose point. The graph increases at a lesser rate deep in the phantom as the number of scattered photons reaching the dose point becomes limited by attenuation. In figure 2-3, SAR/TAR versus field radius, the scatter component again increases rapidly at first and then approaches an asymptotic value. This again, is due to attenuation of the scattered photons. As their distance of origin increases from the central axis, the scattered photons will have a reduced contribution to the SAR. For very large radii a further increase in radius will not alter the SAR.

Figure 2-2 SAR/TAR ratio plotted versus depth in a 10 x 10 cm² Co-60 field.

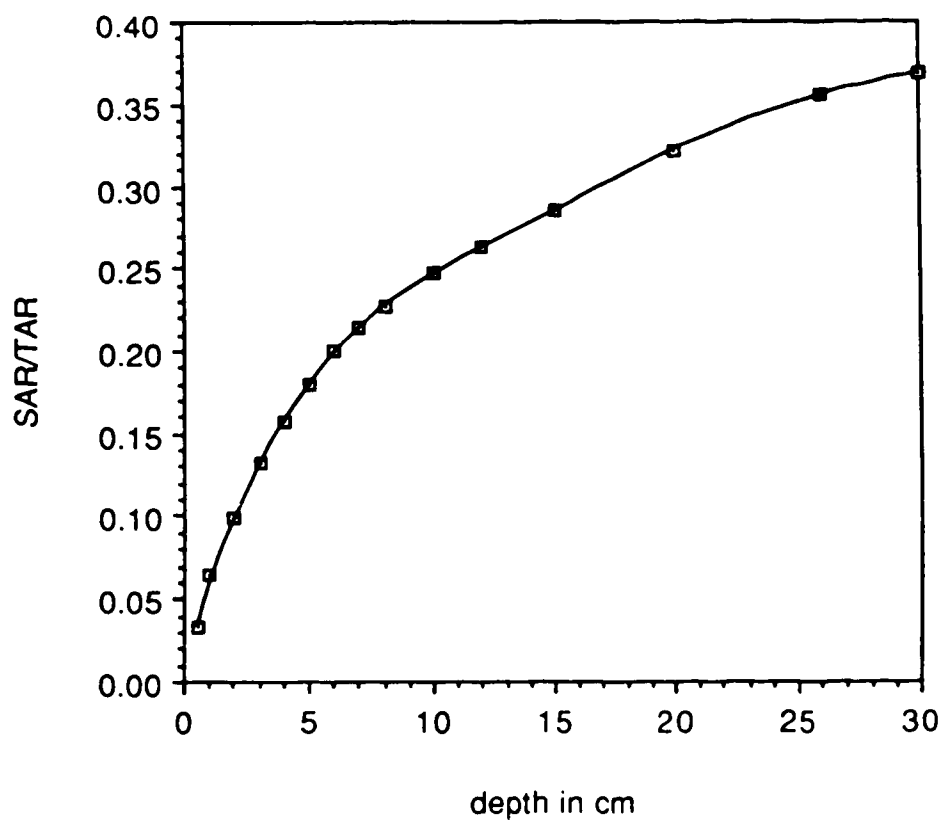
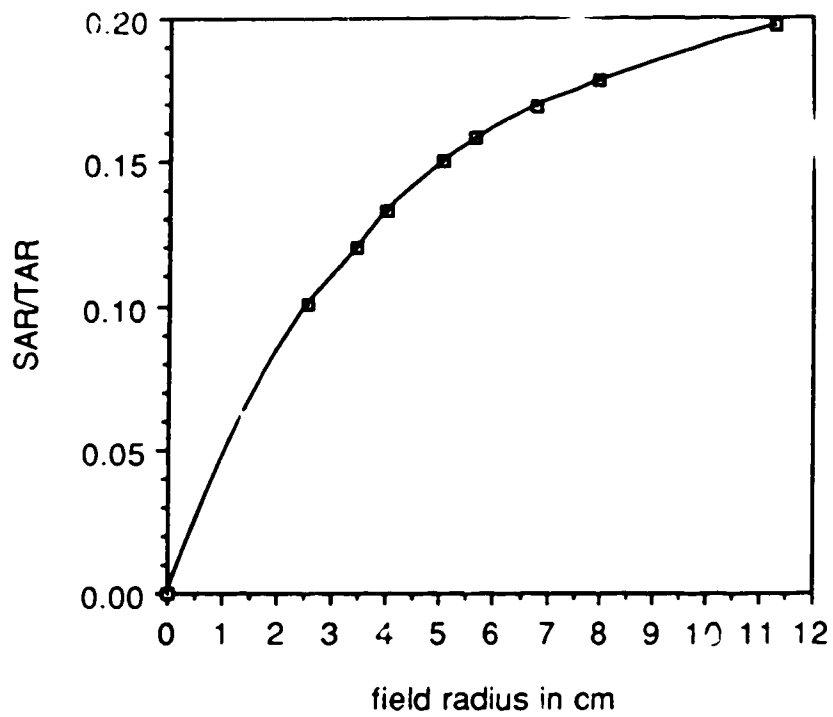


Figure 2-3 SAR/TAR ratio plotted versus field radius at a depth of 4 cm in a Co-60 field.



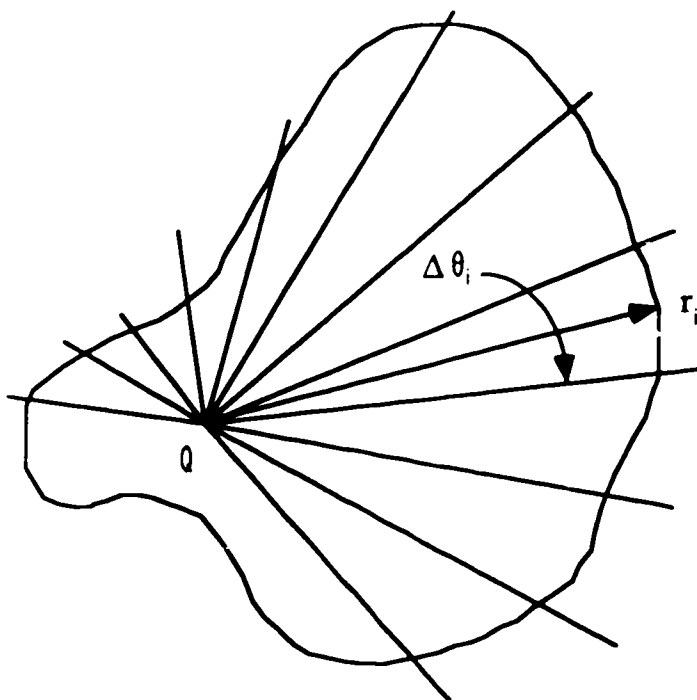
2.12 Sector Integration of Scatter

Since the SAR's are tabulated for fields of varying radii, any shape of field can be divided into circular segments, and the effective scatter air ratio for the field can be found by summing up the SAR's for each segment. This method, developed by Clarkson, can be used to calculate the dose at any point in the field. Figure 2-4 shows how a field might be segmented in such a calculation. The dose at point Q in this field would then be given by the following equation:

$$D_Q = D_{Q, \text{ in air }} \times \left[\text{TAR}(0,d) + \sum_i^n \left\{ \frac{\Delta\theta_i}{2\pi} \text{SAR}(r_i,d) \right\} \right] \quad \text{eqn. 2-4}$$

If there is a shielding block anywhere in the field, then the scatter from the shielded area is reduced by the transmission factor of the block. If the dose point is under the block then the primary is also reduced by the transmission factor.

Figure 2-4 Arbitrary field divided into circular segments whose contribution to the total SAR can be summed up.

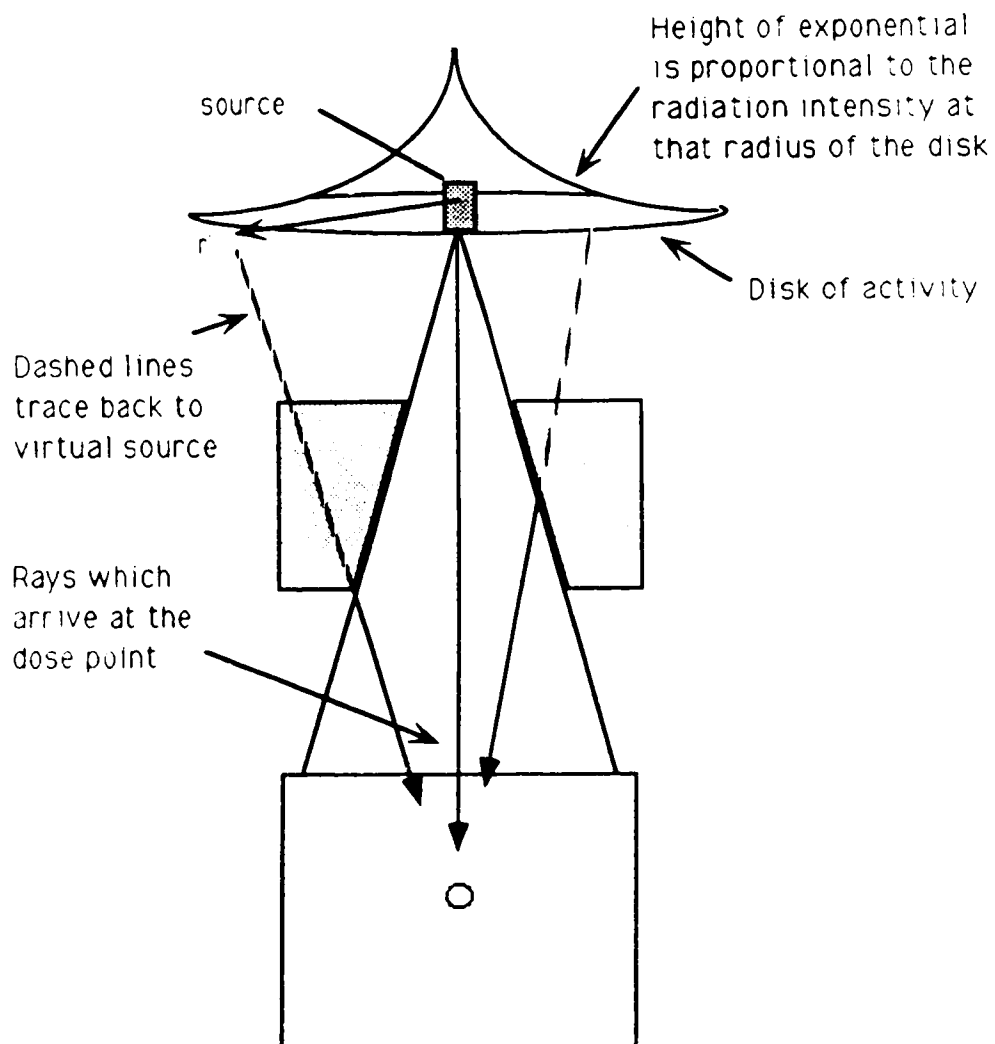


2.13 Sector Integration of the Primary, The Extended Source Model

The sector integration method used to calculate the amount of scatter received at a point is also used to calculate the amount of primary radiation which arrives at a dose point from the source. If the source were an ideal point isotropic emitter, then all areas in the field would be irradiated uniformly. However, in practice, the radiation originates from a small volume within the collimator, and all points in the field do not receive the same amount of radiation from the source. For accelerators, the non-point like source is caused by the fact that the X-rays are produced in the volume of the electron target, and then pass through a beam monitor, a field flattening filter, and the collimator opening. Many of the photons are scattered before they reach the field. In the case of Co-60 machines, the actual physical size of the isotope capsule, as well as scattering, contribute to the broadening of the source effect. Wilkinson, Rawlinson and Cunningham [12] developed the 'extended source model' to correct the Irreg algorithm for the effects of this source broadening on dose calculations. This model is also an important part the Irreg+ program, and a description of it follows.

The extended source model is used to describe the intensity distribution of the primary radiation 'seen' by the dose point looking up the collimator. It describes the source as an infinite disk of activity, with an exponential distribution, shown in figure 2-5. Scattered rays are equivalent to rays originating from virtual sources on the disk, whose intensity is proportional to the value of the exponential function at their point of origin. The exponential shape is verified and parameterized by an analysis of penumbral dose gradients, which will be described in chapter 4.

Figure 2-5 The extended source model developed by Wilkinson, Rawlinson and Cunningham uses an exponential distribution to describe the intensity of the scatter from the collimator.



The radially symmetric activity intensity distribution is given by the following equation:

$$I(r') = \frac{\alpha^2}{2\pi(sd)^2} \exp\left(\frac{-\alpha}{sd} r'\right) \quad \text{eqn. 2-5}$$

Where I is the normalized relative number of photons originating from a unit area at a distance r' from the center of the disk, α is the penumbral parameter, and sd is the physical source diameter. In practice, r' is the radius of a circular sector of the extended source, which results from projecting a sector of radius r from the field, after the field has been divided for a Clarkson's method calculation. A magnification factor relates the two radii, so that r' is given by the following relation,

$$r' = \frac{r (SSD)}{SSD - SDD + d} \quad \text{eqn. 2-6}$$

where SDD is the source to diaphragm or collimator opening distance. When $I(r')$ is integrated over r' and θ , the area of the disk which is visible to the dose point through the collimator opening, it yields eqn. 2-7 for the relative primary fluence:

$$\Phi = \sum_i^{1..n} \frac{\Delta\theta_i}{2\pi} \left[1 - \exp\left(\frac{-\alpha}{sd} r'\right) \left(1 + \frac{\alpha}{sd} r' \right) \right] \quad \text{eqn. 2-7}$$

The source is divided into sectors, of angle $\Delta\theta_i$, which are imaged from the field, and whose contribution is summed up for the total primary calculation. The primary and the scatter sector integrations are done in the same do loop

in the Irreg+ program. When the dose is calculated near the center of a large field, virtually all of the extended source is 'seen', and a large primary dose results. However, if the dose calculation point is near or under a block, or near a field edge, then only part of the source will be 'seen' and contribute, and the primary dose will be reduced.

2.2 Problems with the Irreg+ Algorithm, and need for Experimental Verification

As was mentioned previously, under certain conditions the Irreg+ dose calculations are not within the desired range of accuracy. Clinical experience has shown that when shielding blocks with widths on the order of two centimeters or less are used, the Irreg+ algorithm breaks down for certain depths and energies, and the predicted dose values vary significantly from the measurements. This demonstrates the need for a thorough experimental verification of the Irreg+ calculations under narrow shielding blocks. The next chapter deals with the experimental procedure used to verify the accuracy of the Irreg+ calculations, in an attempt to identify trends in the data which suggest causes for the discrepancies observed, so that corrective measures may be taken

CHAPTER 3

METHOD AND MATERIALS

3.1 Irradiation Conditions

Measurements were made for a wide range of set up conditions, in photon beams of three different energies, Co-60, 6 MV, and 15 MV. Figure 3-1 shows the geometry which was used for making all the measurements. Beginning from the top, we have the radiation source which is either a cobalt capsule, or an accelerator target. The adjustable collimators were used to select two rectangular field sizes, a small 10 x 10 cm², and a large 25 x 25 cm² field. The cerrobend shielding blocks were placed on an acrylic beam accessory tray 55 cm from the source on the cobalt unit, and 54.8 cm from the source on the accelerators. Measurements were made at four depths along the central axis in an almost unit density polystyrene phantom. The cobalt measurements were made with a source to surface distance (SSD) of 80 cm, and those for the accelerator were at 100 cm SSD. The radiation dose measurements were primarily taken with a Capintec model PR-06-C, 0.6 cc farmer type ion chamber, connected to a Capintec 192A electrometer. A diagram of the ion chamber with its dimensions is shown in figure 3-2, the active volume is the tip area, 2.2 cm in length, with an inner diameter of 6.4 mm. A Therados S-9040 p-type diode with a Therados DPD-5 integrator readout was also used as a second dosimeter. Many measurements were taken with both devices for the purpose of comparison.

The blocks were poured from cerrobend alloy such that they were tapered towards the radiation source. This produces better definition of the edges of the shielded area.

Figure 3-1 Experimental Set up

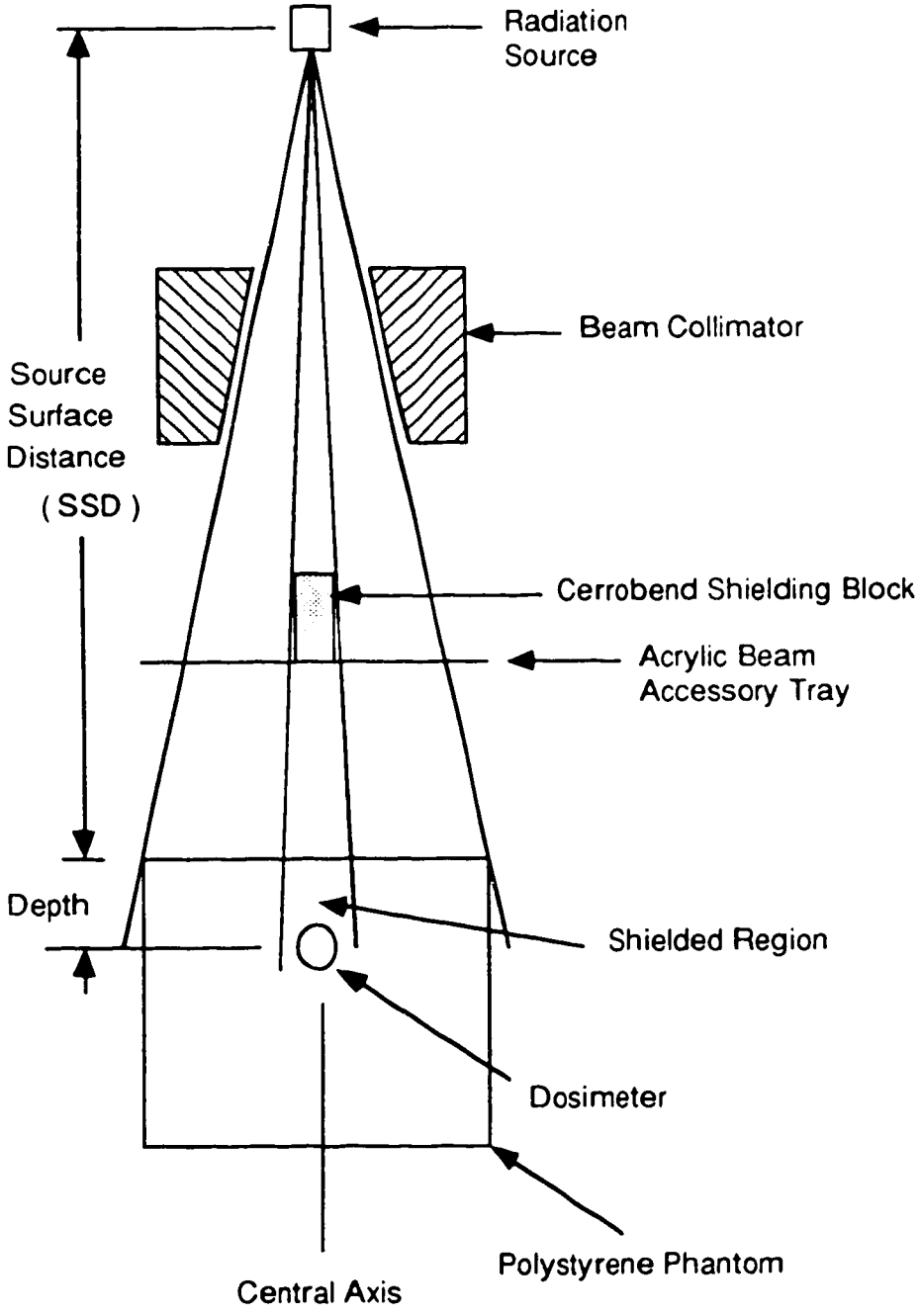
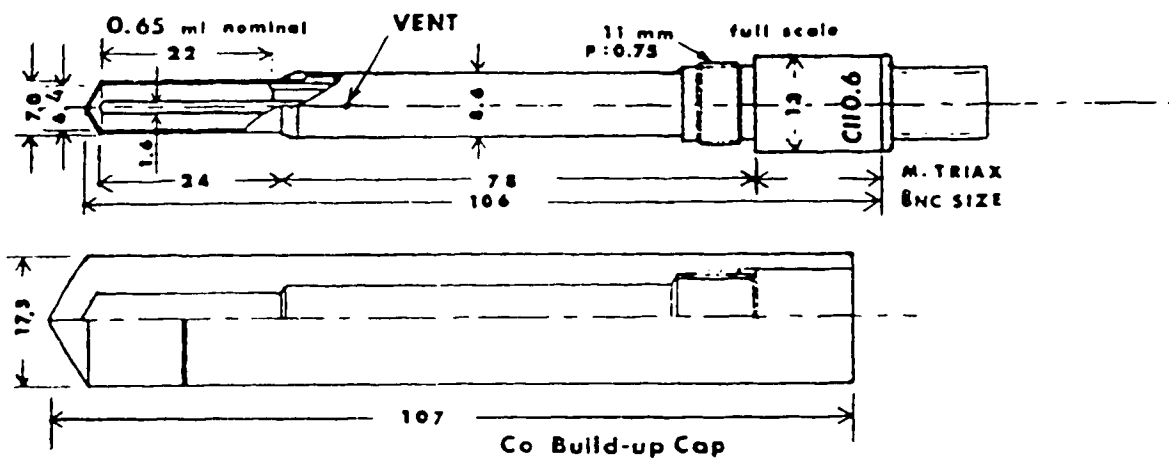


Figure 3-2. Actual size diagram of the Capintec PR-06 ionization chamber and cobalt 60 build up cap [12].



Shielding blocks of many shapes and thicknesses were used for the different energies, their dimensions and shadow sizes are summarized in tables.3-1 to 3-3. The block thicknesses are given in nominal half value layers, or HVL's. This is the thickness of absorber necessary to reduce the fluence of a narrow incident beam to one half of its initial value. The fractional narrow beam primary transmission, T, through a shield, is related to the thickness in half value layers by the following equation:

$$T = \left[\frac{1}{2}\right]^{\# \text{HVL's}} \quad \text{eqn. 3-1}$$

Where #HVL's is the thickness in HVL's of the attenuator. For cerrobend alloy, the narrow beam half value layers for Co-60, 6 MV and 15 MV beams are 1.2, 1.5, and 1.7 cm, respectively.

Table 3-1. Summary of the rectangular, spinal type shielding block thickness, in nominal HVL's, used for the different block base sizes and beam energies.

BASE SIZE	BEAM ENERGY		
	Co-60	6MV	15MV
1 x 7 cm ²	1, 2, 4, 5 HVL's	1, 2, 4, 5 HVL's	1, 2, 4, 5 HVL's
2 x 7 cm ²	1, 2, 4 HVL's	1, 2, 4 HVL's	1, 2, 4 HVL's

The rectangular block sizes were chosen based upon shield sizes which are used clinically to shield the spinal cord. In a study by Mota et. al.

[13] a range of average cord depths and widths of 4.8 ± 1.3 cm and 1.4 ± 0.4 cm respectively, was reported. In order to study conditions of nearly complete occlusion of the beam, a set of thick square shielding blocks was produced which eliminated almost all the primary beam passing through them, so only collimator scatter, and in-phantom scatter was received by dose points beneath them. These occlusion blocks had base sizes of 1.1×1.1 cm², 2.1×2.1 cm², and 4.5×4.5 cm². The first two were 9.8 cm thick, and the latter was 10.4 cm thick. This constant physical thickness produced a different attenuation in each beam energy, therefore the half value thicknesses in each energy are given for the square occlusion blocks in table 3-2.

Table 3-2. Summary of square shielding block thickness, in nominal HVL's, at each energy, for the different block base sizes

BASE SIZE in cm ²	BEAM ENERGY		
	Co-60	6MV	15MV
1.1 x 1.1 and 2.2 x 2.2	8.3HVL's	6.6 HVL's	5.9 HVL's
4.5 x 4.5	8.8 HVL's	6.6 HVL's	6.2 HVL's

The source to accessory tray distances are nearly the same on each machine, however, on the cobalt unit an SSD of 80 cm was used, and on the accelerators a 100 cm SSD was used. This caused a difference in the projected shadow sizes for these two set ups. The shadow sizes are determined by measuring the optical shadow of the block on the phantom

surface. This shadow is produced by a mirror and lamp system positioned in between the primary and secondary collimators such that the light rays trace back to a virtual source at the position of the radiation source. The shadow sizes were also verified by measuring the shadow size the high energy beam produced on radiographic film for the appropriate SSD set up. Table 3-3 lists the shadow sizes of the blocks on the phantom surface for the two set ups.

Table 3-3. Shadow sizes, in cm^2 , of the shielding blocks on the phantom surface for the two source to surface distances used.

Block Base Size, in cm^2	Block Shadow Size in cm^2	
	80 cm SSD	100 cm SSD
1 x 7	1.8 x 12.5	2.0 x 12.75
2 x 7	3.6 x 12.5	4.0 x 12.75
1.1 x 1.1	2.0 x 2.0	2.3 x 2.3
2.1 x 2.1	4.0 x 4.0	4.5 x 4.5
4.5 x 4.5	8.5 x 8.5	9.0 x 9.0

3.2 Measurements

The measurements taken to verify the Irreg+ calculations were as follows. First an ion chamber or diode dose reading was obtained at the desired depth in the phantom without the block in place. This will be called the 'open field dose'. Then, the block was placed on the accessory tray,

centered on the central axis of the beam, and another dose reading, the 'closed field dose'.was taken. The ratio of the two readings, (closed field dose/ open field dose), is the effective transmission, or the fraction by which the open field dose is reduced, when the block is in place. Closed and open field doses were also calculated with the Irreg+ algorithm with parameters selected as to match the experimental conditions. Using a ratio for comparison rather than actual doses eliminated many problems that would have been encountered, such as normalization of the dose measurements, and corrections for pressure and temperature and energy which would have been necessary for the ion chamber readings. In all, measurements were made for nearly 250 different conditions. The results are contained within chapter 4, in tables 4-1, through 4-9.

3.3 Accuracy of the Measurements

The ion chamber is a standard instrument for radiation dose measurement, since its response is highly linear with the amount of dose received, and it has only a small dependence on photon energy. The response is dependent on the ambient pressure and temperature, since these influence the density of the air, but this dependence is removed by using a ratio of two readings, as was done.

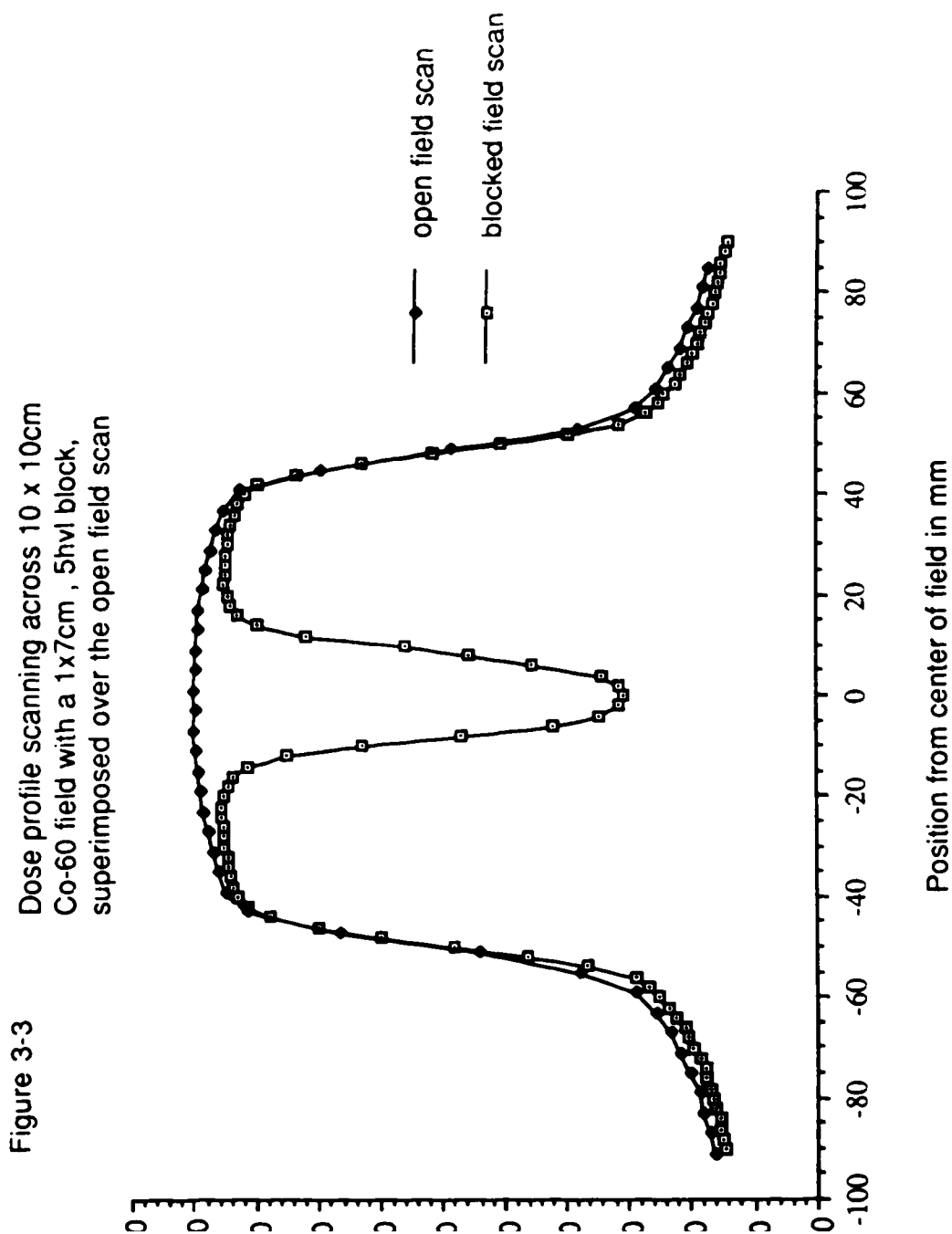
The major sources of error in the effective transmission measurements are caused by positional deviations of the ion chamber or the block from the beam's central axis during set up. Small uncertainties are also present in the depth of the probe, the SSD values, and the radiation output of the accelerators due to statistical variations. However, all these combined, cause only a small amount of error in the effective transmission

measurements. The dose falls off as the inverse square of the source distance, therefore a 3 mm depth variation at a 100 cm source to probe distance (SPD) is going to cause less than a one percent variation in the dose reading. Reproducibility of the measurements showed that the errors caused by positional variations were quite small, and the ion chamber measurements could be considered accurate within $\pm 1\%$.

To ensure that the ion chamber was completely shielded by the blocks for the measurements, a relative dose profile of a blocked field was taken, to determine if the ion chamber would be completely within the width of the umbral region of the shadow. A diode was used on a linear scanner, (Therados RFA7), which moved across a $10 \times 10 \text{ cm}^2$ Co-60 field in air, at an SPD of 80 cm. First an open field scan was taken across the center of the field, then a $1 \times 7 \text{ cm}^2$, 5 HVL shielding block was placed on the accessory tray, and the scan was repeated, with the long axis of the block being perpendicular to the scan direction. Figure 3-3 shows the open and closed field scans superimposed. The maximum open field dose is chosen as 100%, and the other points are normalized to that maximum. The width of the minimum dose, or umbral region below the block is about 10 mm. The inner diameter of the active volume of the ion chamber is 6.5 mm, therefore we can assume that it is completely shielded by the narrowest block.

The films which were used to verify the shadow sizes of the blocks also indicated if the ion chamber would be completely shielded. An optical densitometer was scanned across the films producing curves similar to the blocked field scan of figure 3-3. These displayed for all energies that the $1.1 \times 1.1 \text{ cm}^2$ blocks gave incomplete coverage of the ion chamber, and the coverage of the $2.2 \times 2.2 \text{ cm}^2$ block in the Co-60 field was borderline. All other blocks produced an umbral region large enough to adequately cover

the ion chamber. These results show that for the cases where adequate coverage of the ion chamber occurs, small variations in the block or ion chamber position will have a minor effect the measured results.



3.4 The Diode Response versus the Ion Chamber

3.41 Introduction

As was previously mentioned, a diode was also used to measure many of the effective transmission values. For small geometries, a diode is much better suited for dose measurements than an ion chamber. The diminutive size of the diode produces only a minor perturbation in the radiation field, and allows high spatial resolution to be obtained, which is why it was used for the scans of figure 3-3. Because of the diode's usefulness and the fact that it was the only measuring instrument used under the smallest square shield, its response characteristics were studied in detail. This section will describe these characteristics, as they have a direct bearing on the results of this thesis.

3.42 Angular Dependent Response Variations

It was noted that the diode often gave higher effective transmission readings than the ion chamber, especially for measurements in the lower energy Co-60 beam. It was suspected that the sensitivity of the diode was dependent on its orientation in the beam. This was tested, and verified, but the effect was small. To examine the variation of the response of the diode as a function of the incident angle of the primary radiation, the following experiment was performed. The diode was mounted on a rotatable stand, 1.5 cm below the surface in a water tank, 80 cm SSD, in a 5 x 5 cm² Co-60 field. Readings were taken for 0.5 min. of exposure in the beam, for every

10° interval of rotation of the diode about the axis of its cable. The diode is shown in figure 3-4, with the coordinate system used to describe it. A mark was placed on one side of the diode to arbitrarily label the top. The diode was rotated about the X axis, and a variation in response was obtained versus the incident angle of radiation in the the Y, Z plane.

Figure 3-4 Schematic diagram of the diode showing the coordinate system used to describe the response variations

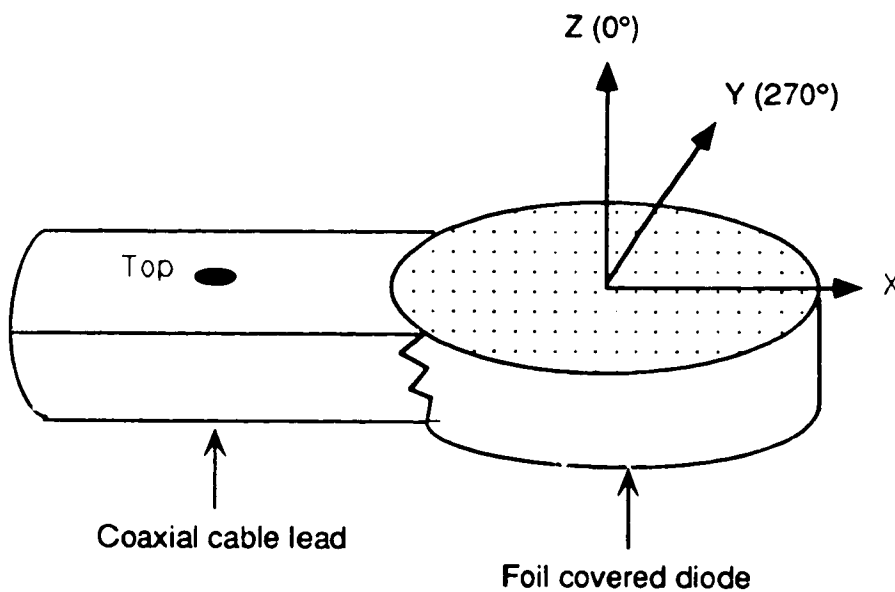
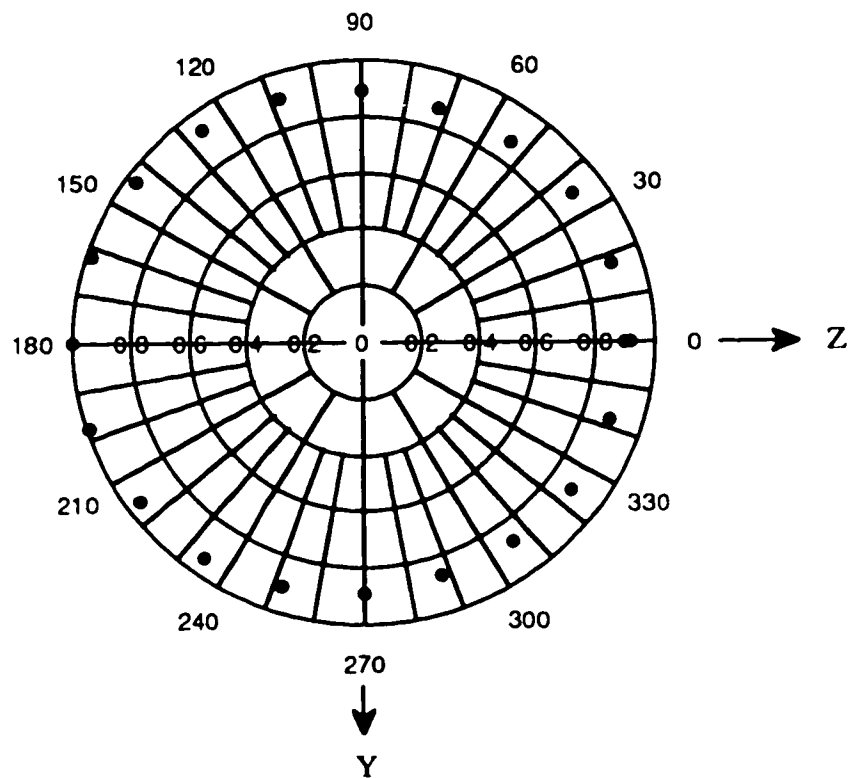


Figure 3-5 Relative response of the diode in water at $D = 1.5$ cm, versus the incident angle in the Z, Y plane of the radiation beam with respect to the \vec{Z} normal.



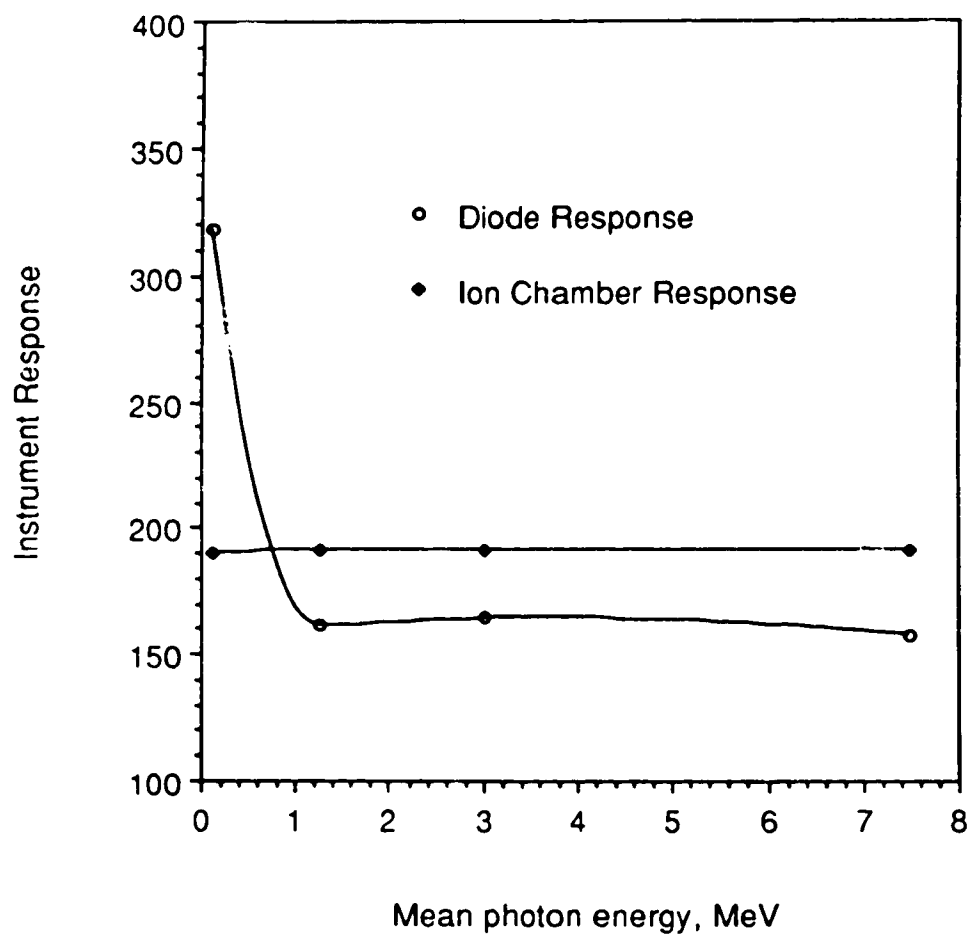
As the diode was rotated a full 360°, an 8% variation in the response was observed. This is shown in figure 3-5, a polar graph in the Y, Z plane, where the radial distance of the points represents the relative response of the diode as a function of the angle. The angular variation results obtained are similar to those reported by Rikner [14]. The cause of this effect is differential attenuation of radiation entering the diode's p-n junction, due to its orientation and differing thicknesses of overlying material. The specifications of the diode were unavailable from the manufacturer, but they are usually constructed with the diode lying on a thin perspex film, with leads attached to a cable, it is then sealed with epoxy, and covered with silver foil [14]. This construction allows for significant variation in the thickness of material overlying the junction.

However, since the orientation of the diode was kept the same for all of the effective transmission measurements, with the 'top' facing the beam, and, since a ratio of two readings was used, it seemed unlikely that directional sensitivity would affect the diode results as much as their observed deviation from the ion chamber values. In fact, when some of the measurements were checked at random, changing the orientation of the diode in the phantom caused only a 1-2% variation in the effective transmission results. Therefore, variations in the directional sensitivity of the diode were not enough to account for the differences in the effective transmission measurements between the diode and the ion chamber, which were as great as 10%. It was then suspected that the response of the diode was also dependent on the photon energy spectrum in the phantom.

3.43 Energy Dependent Response Variations

Since the diode's measurements tended to be higher than the ion chamber's for Co-60, but very close to the ion chamber's values at 15 MV, it appeared the diode was more sensitive to the lower energy radiation. The following experiment was performed to test whether or not the response of the diode was energy dependent. The raw readings of the diode and ion chamber were compared for the same exposure to photons of four energies, 250 KVp, Co-60, 6 MV, and 15 MV. It should be mentioned again that a bremsstrahlung spectrum has mean energy approximately 1/3 to 1/2 of the peak energy, therefore the mean energies of photon beams were ~ 0.125, 1.25, 3.0 and 7.5 MeV. For each energy, except 250 KVp, the diode and the ion chamber were separately placed in the phantom at D_{max} , and irradiated for a time that would produce a dose of 200 cGy. At 250 KVp, the diode and ion chamber were each covered with 0.5 cm of build up material, then irradiated in air. This was done to prevent excessive degradation of the spectrum which would have been caused by low energy backscatter had the measurements been done in the phantom. The raw readings of the diode and ion chamber are plotted versus the approximate mean energy in figure 3-6. At high energies the variation of the raw readings is small for uniform exposure, however, at 125 KVp, the response of the diode doubles. Considering the diode is made from materials which have a relatively high atomic number, Z , compared to the air in the ion chamber, increased absorption of the lower energy radiation results from an increase in the photoelectric cross section, and the diode overresponds to low energy

Figure 3-6 Plot of the response of the diode and the ion chamber versus the mean photon energy for uniform exposure in the beams.



3.44 Conclusions on the Acceptability of the Diode Measurements

It can be seen that the sensitivity of the diode dose increases with lower energies. Under thick shielding blocks most of the dose is due to in phantom scatter which is lower in energy than the primary radiation. Under these conditions, the overresponse of the diode to the low energy scatter increases the closed field dose reading, and consequently, the effective transmission measurements increase. The mean difference between the diode's and the ion chamber's measurements was just under 5%, with a standard deviation of just over 4%. The diode reading was on the high side in most cases. Therefore, in most cases, the diode can be considered accurate to $\pm 5\%$ of the actual value, as measured by the ion chamber. However, measurements in regions dominated by extreme low energy scatter, such as beneath the square occlusion shields in the Co-60 field, the overresponse may be 10% or greater, and strong conclusions should not be based on diode results under these conditions.

CHAPTER 4

RESULTS AND INTERPRETATION

4.0 Results and Interpretation of Data

A large amount of experimental data was obtained over the course of this research project. This chapter will summarize that data, identify the conditions where the Irreg+ calculations are in poor agreement with measurements, and describe steps taken to determine the origin of the discrepancies. After these are identified, further experiments will be described which were used to assess what type of corrective actions should be taken. Finally, corrections will be attempted, and their successfulness evaluated.

4.1 Results

The large amount of data presented here can be cumbersome to the reader, therefore its arrangement will be described as follows. All the measured and calculated effective transmission data is contained in tables 4-1, through 4-9. It is grouped according to energy, such that tables 4-1, 4-2, and 4-3 contain the Co-60 data, tables 4-4, 4-5, and 4-6 give the 6 MV results, and tables 4-7, 4-8, and 4-9 list the 15 MV values. The three tables of each energy group are ordered such that they provide the results for the 2 x 7 cm², the 1 x 7 cm², and the square occlusion blocks respectively. The effective transmission tables for the rectangular shielding blocks are arranged as follow. The base dimensions are listed in the table title, which is followed by a row of column headers for the beam quality, the field size, the block thickness in nominal HVL's, the technique used to obtain the effective transmission values, and the four depths at which these values are compiled. The tables are divided such that the top half contains the values

for the small 10 x 10 cm² field, and the bottom half has the data for the large 25 x 25 cm² field. The data for each field size is divided into sections for each block thickness used. In each of these sections effective transmission values may be given by three or four techniques, an ion chamber measurement, a diode measurement, and two calculations, one labeled 'Irreg+', and the other, 'Modified Irreg+'. Diode measurements were not taken for all of the set up conditions, and are therefore absent from some of the data tables. The rows of values labeled 'Modified Irreg+' are effective transmissions which were generated after some changes were made to the Irreg+ algorithm, in an attempt to improve its accuracy. These modifications, and their effectiveness will be described later in this chapter.

The data table structure for the square occlusion blocks differs somewhat from that of the rectangular shielding blocks. The top of the tables are similar, with headers for beam quality, field size, base size of the blocks, technique for obtaining the effective transmission values, and the four depths at which the values are given. The square block tables are also divided into top and bottom halves for the small and large fields, and these halves are split into sections for each base size of square occlusion block used. The thickness of the blocks in nominal HVL's is given in brackets below the block base size at the beginning of each section. The same four techniques were used to generate the effective transmissions as in the rectangular shielding block tables. Due to the small shadow size of the 1.1 x 1.1 cm² block, the ion chamber could not be adequately shielded, and therefore only diode measurements were attainable beneath it.

Table 4-1 Measured and calculated effective transmissions for a
2 x 7 cm² spinal shield in Co-60 radiation

Beam Quality	Field Size	Block Thickness	Technique	Effective Transmission			
				@ Depth (cm)			
				1.5	5.0	11.5	16.0
Co-60, 10 x 10 cm ²							
		1 HVT	Ion chamber	.500	.525	.561	.578
			Diode	.502	.527	.571	.568
			Irreg+	.525	.539	.558	.570
			Modified Irreg+	.505	.522	.542	.537
		2 HVT	Ion chamber	.270	.300	.350	.374
			Diode	.275	.308	.361	.391
			Irreg+	.287	.307	.336	.355
			Modified Irreg+	.277	.300	.332	.339
		4 HVT	Ion chamber	.096	.133	.188	.228
			Diode	.105	.143	.210	.233
			Irreg+	.108	.135	.170	.193
			Modified Irreg+	.106	.133	.172	.190
Co-60, 25 x 25 cm ²							
		1 HVT	Ion chamber	.527	.561	.619	.655
			Diode	.536	.578	.644	.678
			Irreg+	.543	.568	.618	.648
			Modified Irreg+	.526	.555	.607	.623
		2 HVT	Ion chamber	.309	.357	.439	.488
			Diode	.327	.348	.477	.522
			Irreg+	.315	.353	.428	.470
			Modified Irreg+	.306	.348	.426	.461
		4 HVT	Ion chamber	.147	.204	.304	.364
			Diode	.168	.237	.349	.409
			Irreg+	.144	.193	.286	.338
			Modified Irreg+	.143	.194	.290	.340

**Table 4-2 Measured and calculated effective transmissions for a
1 x 7 cm² spinal shield in Co-60 radiation**

Beam Quality	Field Size	Block Thickness	Technique	Effective Transmission			
				@ Depth (cm)			
				1.5	5.0	11.5	16.0
Co-60, 10 x 10 cm²							
	1 HVT		Ion chamber	.522	.558	.607	.632
			Diode	.530	.567	.611	.634
			Irreg+	.582	.604	.618	.628
			Modified Irreg+	.550	.572	.594	.589
	2 HVT		Ion chamber	.299	.345	.408	.438
			Diode	.307	.359	.420	.452
			Irreg+	.372	.402	.426	.444
			Modified Irreg+	.336	.368	.404	.410
	4 HVT		Ion chamber	.143	.202	.279	.313
			Diode	.149	.219	.287	.323
			Irreg+	.216	.250	.282	.303
			Modified Irreg+	.196	.233	.276	.292
	5 HVT		Ion chamber	.104	.160	.238	.274
			Diode	.109	.177	.253	.290
			Irreg+	.190	.224	.258	.281
			Modified Irreg+	.157	.197	.242	.259
Co-60, 25 x 25 cm²							
	1 HVT		Ion chamber	.558	.600	.665	.699
			Diode	.564	.617	.681	.715
			Irreg+	.599	.626	.673	.699
			Modified Irreg+	.568	.601	.654	.664
	2 HVT		Ion chamber	.347	.407	.496	.546
			Diode	.360	.431	.525	.471
			Irreg+	.399	.440	.508	.546
			Modified Irreg+	.364	.411	.488	.518
	4 HVT		Ion chamber	.203	.307	.386	.441
			Diode	.219	.302	.419	.445
			Irreg+	.248	.301	.385	.433
			Modified Irreg+	.229	.287	.380	.424
	5 HVT		Ion chamber	.166	.240	.351	.411
			Diode	.183	.271	.388	.426
			Irreg+	.233	.276	.324	.414
			Modified Irreg+	.192	.253	.350	.396

Table 4-3 Measured and calculated effective transmissions for square occlusion blocks in Co-60 radiation

Beam Quality	Field Size	Base Size (Thickness)	Technique	Effective Transmission @ Depth (cm)				
				1.5	5.0	11.5	16.0	
Co-60, 10 x 10, 1.1 x 1.1 cm ² (8.3HVL's)				Ion chamber	shadow too small for ion ch.			
				Diode	.113	.200	.302	.248
				Irreg+	.288	.324	.356	.375
				Modified Irreg+	.175	.227	.278	.296
Co-60, 10 x 10, 2.1 x 2.1 cm ² (8.3HVL's)				Ion chamber	.102	.127	.213	.241
				Diode	.056	.118	.206	.346
				Irreg+	.078	.121	.176	.207
				Modified Irreg+	.063	.105	.162	.190
Co-60, 10 x 10, 4.5 x 4.5 cm ² (8.8HVL's)				Ion chamber	.030	.042	.079	.101
				Diode	.027	.046	.088	.108
				Irreg+	.030	.046	.076	.094
				Modified Irreg+	.033	.047	.074	.091
Co-60, 25 x 25, 1.1 x 1.1 cm ² (8.3HVL's)				Ion chamber	shadow too small for ion ch.			
				Diode	.199	.307	.439	.505
				Irreg+	.317	.372	.449	.493
				Modified Irreg+	.210	.281	.381	.428
Co-60, 25 x 25, 2.1 x 2.1 cm ² (8.3HVL's)				Ion chamber	.174	.202	.332	.387
				Diode	.131	.219	.354	.420
				Irreg+	.117	.183	.295	.356
				Modified Irreg+	.101	.167	.282	.342
Co-60, 25 x 25, 4.5 x 4.5 cm ² (8.8HVL's)				Ion chamber	.070	.114	.204	.257
				Diode	.085	.139	.241	.298
				Irreg+	.070	.114	.208	.264
				Modified Irreg+	.073	.115	.208	.259

**Table 4-4 Measured and calculated effective transmissions for a
2 x 7 cm² spinal shield in 6 MV radiation**

Beam Quality	Field Size	Block Thickness	Technique	Effective Transmission			
				Dmax	1.5	5.0	11.5
6 MV, 10 x 10 cm²							
	1 HVT		Ion chamber	.488	.504	.533	.548
			Irreg+	.516	.529	.547	.558
			Modified Irreg+	.483	.498	.520	.531
	2 HVT		Ion chamber	.262	.280	.318	.337
			Irreg+	.275	.294	.322	.338
			Modified Irreg+	.258	.280	.310	.327
	4 HVT		Ion chamber	.113	.126	.168	.188
			Irreg+	.094	.118	.153	.174
			Modified Irreg+	.116	.141	.178	.197
6 MV, 25 x 25 cm²							
	1 HVT		Ion chamber	.509	.532	.518	.604
			Irreg+	.527	.545	.588	.612
			Modified Irreg+	.495	.515	.562	.589
	2 HVT		Ion chamber	.289	.327	.384	.420
			Irreg+	.291	.317	.383	.400
			Modified Irreg+	.275	.303	.372	.409
	4 HVT		Ion chamber	.163	.177	.248	.290
			Irreg+	.114	.147	.228	.273
			Modified Irreg+	.136	.174	.251	.295

**Table 4-5 Measured and calculated effective transmissions for a
1 x 7 cm² spinal shield in 6 MV radiation**

Beam Quality	Field Size	Block Thickness	Technique	Effective Transmission			
				Dmax	1.5	5.0	11.5
6 MV, 10 x 10 cm ²							
	1 HVT		Ion chamber	.506	.526	.560	.582
			Irreg+	.543	.558	.579	.592
			Modified Irreg+	.506	.522	.546	.558
	2 HVT		Ion chamber	.282	.311	.358	.381
			Irreg+	.314	.338	.370	.389
			Modified Irreg+	.293	.317	.350	.369
	4 HVT		Ion chamber	.112	.147	.198	.227
			Irreg+	.144	.172	.213	.236
			Modified Irreg+	.140	.169	.210	.231
	5 HVT		Ion chamber	.089	.126	.180	.204
			Irreg+	.114	.145	.196	.210
			Modified Irreg+	.129	.159	.200	.223
6 MV, 25 x 25 cm ²							
	1 HVT		Ion chamber	.544	.575	.619	.644
			Irreg+	.580	.600	.642	.665
			Modified Irreg+	.517	.539	.588	.614
	2 HVT		Ion chamber	.315	.363	.439	.477
			Irreg+	.330	.361	.427	.464
			Modified Irreg+	.309	.340	.409	.447
	4 HVT		Ion chamber	.159	.211	.296	.341
			Irreg+	.163	.201	.285	.331
			Modified Irreg+	.160	.198	.282	.328
	5 HVT		Ion chamber	.136	.193	.281	.325
			Irreg+	.135	.175	.260	.309
			Modified Irreg+	.149	.187	.273	.320

Table 4-6 Measured and calculated effective transmissions for square occlusion blocks in 6 MV radiation

Beam Quality	Field Size	Base Size (Thickness)	Technique	Effective Transmission			
				Dmax	1.5	5.0	@ Depth (cm) 11.5 16.0
6 MV	10 x 10	1.1 x 1.1 cm ² (6.6 HVL's)	Ion chamber	shadow too small for ion ch.			
			Diode	.095	.149	.224	.257
			Irreg+	.139	.179	.228	.257
			Modified Irreg+	.142	.179	.231	.259
			<hr/>				
6 MV	10 x 10	2.1 x 2.1 cm ² (6.6 HVL's)	Ion chamber	.043	.067	.122	.148
			Diode	.043	.081	.137	.165
			Irreg+	.048	.083	.134	.161
			Modified Irreg+	.047	.077	.124	.151
			<hr/>				
6 MV	10 x 10	4.5 x 4.5 cm ² (7.1 HVL's)	Ion chamber	.024	.028	.040	.050
			Diode	.025	.033	.046	.060
			Irreg+	.024	.030	.045	.053
			Modified Irreg+	.032	.035	.045	.054
			<hr/>				
6 MV	25 x 25	1.1 x 1.1 cm ² (6.6 HVL's)	Ion chamber	shadow too small for ion ch.			
			Diode	.150	.229	.336	.388
			Irreg+	.159	.207	.302	.352
			Modified Irreg+	.163	.210	.305	.356
			<hr/>				
6 MV	25 x 25	2.1 x 2.1 cm ² (6.6 HVL's)	Ion chamber	.090	.125	.217	.262
			Diode	.093	.153	.252	.301
			Irreg+	.071	.117	.217	.270
			Modified Irreg+	.070	.111	.207	.261
			<hr/>				
6 MV	25 x 25	4.5 x 4.5 cm ² (7.1 HVL's)	Ion chamber	.062	.077	.135	.170
			Diode	.068	.102	.165	.203
			Irreg+	.048	.067	.136	.176
			Modified Irreg+	.055	.071	.136	.172
			<hr/>				

Table Measured and calculated effective transmissions for a
2 x 7 cm² spinal shield in 15 MV radiation

Beam Quality	Field Size	Block Thickness	Technique	Effective Transmission			
				Dmax	3.0	5.0	11.5
15 MV, 10 x 10 cm ²							
		1 HVT	Ion chamber	.502	.500	.510	.516
			Diode	.500	.497	.511	.523
			Irreg+	.516	.521	.528	.558
			Modified Irreg+	.512	.517	.525	.531
		2 HVT	Ion chamber	.251	.249	.266	.275
			Diode	.253	.251	.267	.275
			Irreg+	.274	.281	.291	.308
			Modified Irreg+	.267	.275	.285	.294
		4 HVT	Ion chamber	.084	.083	.100	.111
			Diode	.084	.082	.107	.119
			Irreg+	.092	.103	.115	.125
			Modified Irreg+	.103	.113	.126	.137
15 MV, 25 x 25 cm ²							
		1 HVT	Ion chamber	.526	.516	.536	.548
			Diode	.523	.519	.542	.562
			Irreg+	.528	.533	.549	.563
			Modified Irreg+	.525	.531	.546	.561
		2 HVT	Ion chamber	.288	.274	.302	.322
			Diode	.284	.278	.313	.339
			Irreg+	.293	.301	.323	.346
			Modified Irreg+	.286	.294	.318	.341
		4 HVT	Ion chamber	.128	.114	.147	.171
			Diode	.126	.122	.160	.182
			Irreg+	.116	.126	.154	.182
			Modified Irreg+	.126	.137	.165	.193

Table 4-8 Measured and calculated effective transmissions for a
1 x 7 cm² spinal shield in 15 MV radiation

Beam Quality	Field Size	Block Thickness	Technique	Effective Transmission			
				Dmax	3.0	5.0	11.5
15 MV, 10 x 10 cm ²							
		1 HVT	Ion chamber	.518	.521	.539	.549
			Irreg+	.542	.549	.554	.559
			Modified Irreg+	.523	.530	.536	.541
		2 HVT	Ion chamber	.301	.311	.336	.348
			Irreg+	.313	.324	.331	.339
			Modified Irreg+	.311	.322	.329	.337
		4 HVT	Ion chamber	.144	.157	.185	.196
			Irreg+	.141	.156	.166	.175
			Modified Irreg+	.159	.174	.182	.190
		5 HVT	Ion chamber	.108	.114	.140	.156
			Irreg+	.112	.127	.137	.147
			Modified Irreg+	.130	.145	.153	.164
15 MV, 25 x 25 cm ²							
		1 HVT	Ion chamber	.539	.543	.573	.586
			Irreg+	.554	.562	.576	.589
			Modified Irreg+	.536	.543	.558	.573
		2 HVT	Ion chamber	.334	.341	.383	.402
			Irreg+	.331	.342	.364	.384
			Modified Irreg+	.329	.340	.361	.381
		4 HVT	Ion chamber	.185	.194	.237	.265
			Irreg+	.164	.178	.204	.231
			Modified Irreg+	.181	.195	.220	.246
		5 HVT	Ion chamber	.149	.153	.197	.225
			Irreg+	.135	.150	.177	.204
			Modified Irreg+	.153	.167	.193	.220

Table 4-9 Diode and calculated effective transmissions for square occlusion blocks in 15 MV radiation

Beam Quality	Field Size	Base Size (Thickness)	Technique	Effective Transmission			
				Dmax	3.0	5.0	11.5
15 MV	10 x 10	1.1 x 1.1 cm ² (5.9 HVL's)	Ion chamber	shadow too small for ion ch.			
			Diode	.136	.154	.193	.213
			Irreg+	.141	.162	.171	.182
			Modified Irreg+	.153	.174	.184	.194
15 MV	10 x 10	2.1 x 2.1 cm ² (5.9 HVL's)	Ion chamber	.064	.063	.089	.106
			Diode	.054	.057	.089	.107
			Irreg+	.053	.067	.084	.098
			Modified Irreg+	.064	.077	.094	.109
15 MV	10 x 10	4.5 x 4.5 cm ² (6.2 HVL's)	Ion chamber	.030	.027	.034	.038
			Diode	.028	.026	.033	.040
			Irreg+	.029	.030	.036	.040
			Modified Irreg+	.049	.050	.055	.060
15 MV	25 x 25	1.1 x 1.1 cm ² (5.9 HVL's)	Ion chamber	shadow too small for ion ch.			
			Diode	.190	.199	.259	.288
			Irreg+	.165	.185	.212	.239
			Modified Irreg+	.177	.179	.223	.250
15 MV	25 x 25	2.1 x 2.1 cm ² (5.9 HVL's)	Ion chamber	.117	.099	.144	.172
			Diode	.102	.100	.156	.185
			Irreg+	.079	.093	.128	.163
			Modified Irreg+	.089	.104	.138	.172
15 MV	25 x 25	4.5 x 4.5 cm ² (6.2 HVL's)	Ion chamber	.073	.056	.083	.101
			Diode	.071	.065	.099	.118
			Irreg+	.056	.057	.082	.107
			Modified Irreg+	.075	.076	.101	.126

4.2 Discussion of the Results

A few points should be made with regard to the Irreg+ algorithm, and shielding blocks, before the discussion. The purpose of the Irreg+ algorithm is to correct the dose calculation at a point for scattered radiation received from within the field, and from the collimator. This correction is far superior to a simple primary attenuation calculation which does not correct for scatter. In terms of the percent errors between the Irreg+ calculations and the measurements, some apparently large discrepancies occur in the data. However, in most cases these are large errors in greatly reduced doses behind the thick shielding blocks, and the clinical effects of these errors may indeed be below the threshold of measurement. Since the term 'effective transmission' can be rather cumbersome, 'dose ratio' may be used in its place, since the ratio of the the closed to open field doses is proportional to the effective transmission.

A quantity which will be used to indicate the accuracy of the Irreg+ calculations is the root mean square (rms) error. This is calculated with the following equation:

$$\text{rms error} = \frac{1}{n} \sqrt{\sum_i^n (x_{i,\text{calc}} - x_{i,\text{meas}})^2} \quad \text{eqn. 4-1}$$

where $x_{i,\text{calc}}$ and $x_{i,\text{meas}}$ are corresponding calculated and measured effective transmission values in a data table of n elements. The rms error indicates an average absolute difference between the calculated and measured effective transmission values in the data table it is quoted for.

4.21 Trends in the Co-60 Data

The Irreg+ calculations for the effective transmissions under the 2×7 cm² spinal shields in Co-60 radiation, as seen in table 4-1, were in good agreement with the measurements. The root mean square difference between the measured and the calculated dose ratios, is found to be only 0.014. This means the rms error in the dose under the block is 1.4% of the open field dose. The largest error occurred 16 cm deep in the phantom, under the 4 HVT block in the small field, where Irreg+ predicted a dose ratio of 0.193, and 0.228 was measured. This is a 15% difference between the measurement and the calculation, however, the discrepancy is only 3.5% of the open field dose. In the above conditions, a simple primary transmission calculation would yield a dose ratio of 0.063, so it can be seen that Irreg+ models the scatter well, producing a result which is much closer to the measured value.

When the narrower 1×7 cm² shielding blocks were used in the cobalt field, (table 4-2), the Irreg+ effective transmission predictions did not agree as well with the measurements, as the rms difference between the two increased to 0.039. Underneath the narrower blocks Irreg+ appeared to have some difficulties predicting the dose ratio at shallow depths. Most of the larger errors were dose ratio overpredictions at depths of 1.5 and 5.0 cm, in both the small and large fields. However, at depths of 11.5 and 16.0 cm, the Irreg+ values were much better, with some being exactly the same as their measured counterparts.

Due to the uncertainties of measurement involved, the square block Co-60 data, (table 4-3), must be interpreted carefully. Since the ion chamber does not fit in the shadow of the 1.1×1.1 cm² block, and it just fits in the

shadow of the 2.1 x 2.1 cm² block near the surface, only the diode can be relied on for measurements in these conditions. Under the square occlusion shields however, most of the primary has been eliminated from the beam, and the diode 'sees' only scattered radiation. As was mentioned in chapter 3, these are the conditions where the diode shows a spectrally dependant change in response, and its measurements should only be considered accurate within 10%.

The square occlusion shields are also the most difficult test for the Irreg+ algorithm, as there is virtually no primary transmission through them, and all the dose is due to scatter. In spite of these difficulties however, reasonable agreement between the measurements and the calculations was obtained. The rms error is 0.069, but is skewed by four large values, most of the other twenty errors are all less than 0.040. Again, as with the 1 x 7 cm² blocks, the larger errors occur near the surface, and better agreement is obtained deeper in the phantom. For example, in the large field under the 1.1 x 1.1 cm² block, Irreg+ predicts an effective transmission of 0.317 at 1.5 cm compared to a measurement of 0.199, however at 16.0 cm deep, Irreg+ predicted 0.493 which is remarkably close under these conditions to the measured value of 0.505. While, Irreg+ does have some trouble spots in the Co-60 data, in general it appears to be modeling the scatter well.

4.22 Trends in the 6 MV Data

The Irreg+ performance in the 6 MV data generally showed an improved agreement with measurements of the Co-60 data. Under the 2 x 7 cm² shields, (table 4-4), the rms difference between the calculated and measured effective transmissions is 0.019, with the worst case being a 0.054

underprediction 1.5 cm deep, in the large field, below the 4 HVT block. A small improvement with depth occurs, but the effect is not as obvious as with the cobalt data. All the 1 HVT block values are overpredicted, and all the 4 HVT block values are underpredicted by Irreg+. Both types of errors occur under the 2 HVT blocks.

When the smaller 1 x 7 cm² shields were used, (table 4-5), the rms error of the calculations increased slightly to 0.020. In the small field, there is a trend towards dose ratio overpredictions near the surface which improve with depth, but in the large field, a trend is difficult to establish.

Underneath the square shielding blocks in 6 MV, (table 4-6), the problems of measurement encountered with Co-60, were present, but not as severe. There was an improved agreement between the ion chamber and the diode measurements, and some trends in the accuracy of the calculations were discernable. The rms difference was only 0.018, much better than with cobalt. The largest error was a 0.044 overprediction in the small field under the smallest occlusion shield, 1.1 x 1.1 cm² , at 1.5 cm deep in the phantom, however, at 16 cm deep, Irreg+ agreed exactly with the effective transmission measurement made with the diode. The other errors in the small field were minor dose ratio overpredictions, and some underpredictions also occurred in the large field. In general, though, Irreg+ performed very well considering the conditions.

4.23 Trends in the 15 MV Data

In general Irreg+ performed well for dose calculations at 15 MV, under the 2 x 7 cm² shielding blocks, (table 4-7). The rms difference between the effective transmission measurements and calculations is 0.020, with no

extreme deviations. There was no noticeable change in accuracy with depth, as was observed for the other energies. All but one of the errors were dose ratio overpredictions, with the single underprediction occurring at D_{max} in the large field, under the 4 HVT block.

When narrower $1 \times 7 \text{ cm}^2$ shielding blocks were used, in the 15 MV beam, (table 4-8), the accuracy of Irreg+ improved slightly, with the rms error being only 0.016. This was unexpected since with the other two energies, the accuracy of Irreg+ decreased for the narrower blocks. Beneath the 1 and 2 HVT blocks, dose ratio overpredictions prevailed, while under the 4 and 5 HVT blocks, underpredictions were dominant. Again, the accuracy of the calculations did not appear to change with depth.

Beneath the square occlusion shields in 15 MV, (table 4-9), reasonable agreement between the diode and ion chamber was obtained, and an rms error of 0.019 occurred between the Irreg+ calculations and the dose ratio measurements. The largest errors of .047 and .049 were under the smallest shield in the large field where at depths of 11.5 and 16.0 cm Irreg+ predicted dose ratios of .259 and .288 respectively while values of .212 and .239 were measured. Again, this is a region of extreme scatter, where a simple primary calculation would give a dose ratio of only .017, thus, by considering the scatter, Irreg+ provides a much better estimate of the ratio of the blocked to open field dose.

4.3 Clinical Significance of the Discrepancies

Although some large discrepancies were observed, a few comments are needed in order to give them more meaning and to put them into clinical perspective. One notable point is that a majority of the discrepancies are

dose overpredictions under thick shielding blocks. These are errors on the 'safe side', since the shielded area is actually receiving a lower dose than calculated by Irreg+. However in some cases only partial shielding is employed, and it is desirable to keep the shielded dose at a prescribed level. Examples of this are the use of partial lung shields in the treatment of Hodgkins disease and partial kidney shields in the treatment of ovarian cancer. In these scenarios, dose underpredictions and overpredictions are of concern. It should be known if the amount of overdosing or underdosing due to erroneous calculations may be enough to cause complications in treatment. In other words, a reasonable limit of certainty must be chosen within which the Irreg+ dose calculations should be contained, in order to deliver a required quality of treatment in these circumstances.

Although some of the percent discrepancies between calculated and measured dose ratios in the data are very large, it must be kept in mind that most of these large percent errors occurred in what are greatly reduced absolute doses. It is necessary therefore to introduce some guidelines on how large a discrepancy can be before it should be considered clinically significant. According to the conclusions of the ICRU #24 Report [2], as was mentioned earlier, the target volume dose should be delivered to an accuracy of $\pm 5\%$, with $\pm 3\%$ of this error allowed in the computation stage of the treatment planning. This is the accuracy required for the target volume, which receives the greatest dose. This margin is to ensure tumor control, and prevent complications of surrounding healthy tissue.

Assuming the target is in the open field, adjacent to a shielded point, an error of 3% in the target dose corresponds to a variation of 3% in the open field dose. This is also equivalent to a variation of 0.030 in the open field transmission. Therefore, a discrepancy of 0.030 in the effective

transmission to the shielded point, will give an absolute uncertainty in the shielded dose which is 3% of the open field, or target dose. For example, if 3% of the target dose at some depth is X Grays, and an adjacent location is shielded, then a 0.030 error in the effective transmission under the shield also yields a variation of X Grays in the shielded dose at that depth. Since a variation of X Grays is a tolerable amount to the tissue around the target volume, it should be a tolerable amount to the shielded region in most cases. Therefore, with this reasoning, it is absolute differences greater than ± 0.030 between the measured and the calculated effective transmissions that will be considered significant discrepancies and of concern in this thesis.

The local discrepancy, or percent difference between a calculated and measured effective transmission will always be greater than 3% if there is an absolute difference of 0.030 between the two values. Therefore, the chosen guideline for a significant discrepancy is a flag which indicates areas where calculational shortcomings will lead to errors greater than 3% in the dose delivered under the shield. Due to the nature of the observed discrepancies, it is difficult to make a statement on the overall local accuracy of the Irreg+ algorithm. However, the discrepancies can be classified, explained, and commented on according to the conditions in which they occur, thereby putting them into clinical perspective. Table 4-10 highlights areas of greatest discrepancy between Irreg+ and measurement for each depth, block thickness, and energy. Of the 45 discrepancies encountered, out of a total of 240 measurements, 19 occurred under the square occlusion blocks which were greater than 5 HVL's thick, and 12 were observed under the 4 and 5 HVL blocks.

Table 4-10 Frequency of discrepancies exceeding 0.030 between the Irreg+ calculations and the measurements for all the data tables. The symbols are tallies for the discrepancies observed at each energy, X for Co-60, O for 6MV, and I for 15MV, for the given depth and block thickness.

Block Thickness HVL	Depth of measurements, cm			
	1.5	5.0	11.5	16.0
1	XX OO	X O		
2	XX O	XX 		
4	XX OO	X		X
5	XX	XX		
>5	XXX O *	XX	XXX O 	XXX O
Total	19	10	6	10

* depth for this 15 MV value is 3.0 cm

As was described in chapter 3, many of the first 19 discrepancies can be accounted for by the difficulties of measurement under the small square shields. Even so, there remain 31 discrepancies under very thick shielding blocks. These blocks have uses such as complete spinal shielding, where they greatly reduce the given dose, so that even with large local errors the dose is still greatly reduced from the open field, and unacceptable overdoses should not occur in most cases.

This leaves 14 discrepancies under the 1 and 2 HVL shields, 11 of which were under the narrower 1 cm wide blocks. The accuracy required under blocks of these thicknesses is of a more critical nature, since they are typical for applications such as partial kidney shielding in the treatment of ovarian cancer, where the shielded dose must be kept within 3% of the desired value. Irreg+ did have difficulties in this region, since 14 of 96 effective transmission calculations under the 1 and 2 HVL blocks had discrepancies greater than 0.03 from the measurements. Since most of these occurred under 1 cm wide blocks, Irreg+ results under these blocks should be used with caution, but results under the 2 cm wide partial shields can be used with confidence. It was found that most the 14 discrepancies did not arise from the Irreg+ algorithm, but rather from difficulties in fabricating cerrobend blocks, and an inability to accurately determine their narrow beam transmissions, which are important parameters the user must enter into the Irreg+ program. By the use of more appropriate values, 6 of these discrepancies were corrected, and of the remaining 8, 5 occurred in the Co-60 calculations. The cause of the discrepancies in the Co-60 calculations is predominantly due to a poor extended source model, which will be discussed in the following sections. In general, Irreg+ performs well, except for Co-60 where there are some notable exceptions.

4.4 Sources of Error in the Irreg+ Algorithm

This section will further examine the Irreg+ dose calculation method described in chapter 2, and identify the causes of the discrepancies in the calculations that were observed. When the large discrepancies were discovered in the Co-60 data, the scatter component of the calculation was

suspect. It was thought that the algorithm may have been interpolating the scatter air ratios incorrectly for the small radii segments of the shielded area, thus computing an incorrect scatter component of the dose. This however was not the cause of the overpredictions. Use of the interactive fortran debugger showed that the scatter dose was correct, and that the primary component of the dose calculation was erroneous. The primary component was too large in most cases, which led to the dose ratio overpredictions of Irreg+ in the Co-60 data.

The primary component of the dose as described in section 2.13 is calculated by integrating the area of the extended source seen by the dose point. The error in the primary dose calculation was traced to an incorrect parameterization of the extended source model, such that too much of the source was being 'seen' by points under the small shields. When the extended source model was verified for Co-60 by an analysis of the penumbral dose gradients, it was determined that the source intensity distribution was incorrectly parameterized. The details of this procedure will be described in section 4.5.

The extended source parameters were not verified for the 6 and 15 MV calculations, as the process was very time consuming due to the large number of measurements required. However, another source of discrepancy was determined to be affecting these results, and also those of Co-60. As previously stated, the narrow beam transmission of a shielding block is entered into the Irreg+ program, which uses it in both components of the dose calculation. If the value entered is not the true transmission, then discrepancies between the measured and calculated doses will arise. Measurements of the physical thickness of the blocks showed that deviations up to 2 mm occurred from what their thickness should have been

for requested number of half value layers. This would cause a negligible difference in the primary transmissions of the 4 and 5 HVL blocks, but in the 1 and 2 HVL blocks, these thickness variations could create differences up to 4% in the narrow beam transmission. This in turn could translate to a discrepancy of 0.040 between the measured and calculated effective transmissions. Also, internal flaws such as bubbles within the blocks may lead to differences between their true and expected narrow beam transmissions.

To determine how correct the block transmissions being entered into the Irreg+ program were, a series of 'in air' transmission measurements were performed. These were not rigorous narrow beam transmission measurements as the cobalt collimators would only close enough to form a 4.0 x 4.0 cm² field at 80 cm SSD. The collimators on the 6 and 15 MV machines were closed to the width of the blocks. Ion chamber measurements were taken in air, with and without the blocks in place. The ratios of the two readings are estimates of the narrow beam transmission of the blocks. The nominal primary transmissions of the blocks, which were used in Irreg+, are listed in table 4-11 along with their associated measured estimates for each energy. For the square occlusion blocks there are three nominal primary transmission values listed, these are for Co-60, 6 MV and 15 MV respectively, since the same block was used for all energies.

These measured estimates of the narrow beam transmissions of the shielding blocks were used in the Modified Irreg+ calculations for all energies. The number of discrepancies observed under the 1 and 2 HVL blocks in the modified data was reduced from 14 to 8, of which 5 were in the Co-60 data. For the Co-60 Modified Irreg+ calculations a different experimentally verified extended source parameter was used, this also

contributed partially to reducing the number discrepancies for that energy. The remaining discrepancies demonstrate the limitations of the extended source model, and possible errors in measurement.

Table 4-11 Measured primary transmission estimates of the shielding blocks used, and the transmissions expected from the nominal HVL's of the blocks.

Block Type	Nominal Narrow beam Transmission	Measured Narrow Beam Transmission Estimates		
		Co-60	6 MV	15 MV
2 x 7 cm ²	.500	.484	.463	.494
	.250	.245	.229	.239
	.063	.066	.067	.069
1 x 7 cm ²	.500	.491	.464	.484
	.250	.257	.233	.240
	.063	.090	.081	.073
	.031	.047	.037	.041
1.1x1.1	.003, .010, .017	*	.022	.037
2.1x2.1	.003, .010, .017	.012	.015	.028
4.5x4.5	.002, .007, .014	.007	.018	.033

* indicates measurement not possible, the shadow size was too small for the ion chamber to be completely shielded.

4.5 Verification of the Extended Source Parameter, α .

Consider the extended source described in section 2.13. In order to verify the intensity function, a method of measuring $\frac{d\Phi}{dA}$, the relative fluence per unit area of the source is necessary. This can be done indirectly, as was described by Wilkinson [11]. This method was used to verify the extended source function for the Theratron 780 Co-60 unit, and the procedure will now be explained.

Consider a point at the beam edge, which by definition is exposed to only one half of the source, shown in fig 4-1. A small increment in field size in the x direction will 'uncover' a narrow strip of the extended source which passes through the center, i.e. through the intensity function $I(r)$ at $r=0$. The increment in dose, ΔD , to the point P, caused by uncovering this strip will then be the line integral of this intensity function over a distance equal to the field width. If the field is sufficiently large, and the point considered is a long way from the corners, then for all practical purposes, this integral is over $\pm \infty$, in equation form that is;

$$\Delta D = \Delta x \int_{y_2}^{y_1} I(y) dy \quad \text{eqn. 4-2}$$

where $y_1 = +\infty$ and $y_2 = -\infty$. In the limit as $\Delta x \rightarrow 0$, this becomes the derivative, or gradient of the dose in the x direction at the point P.

$$\frac{dD_p}{dx} = \int_{y_2}^{y_1} I(y) dy \quad \text{eqn. 4-3}$$

Figure 4-1. Dose point, P, shown at the edge of the field, the half rings surrounding it represent lines of equal intensity of the extended source which the point 'sees' looking up the collimator.

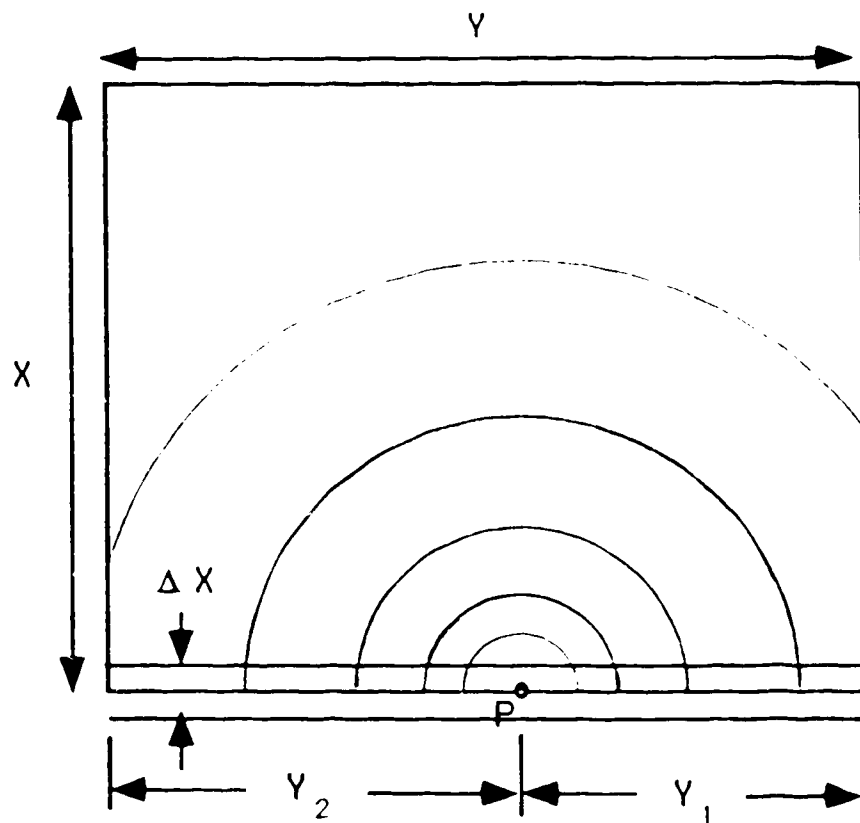
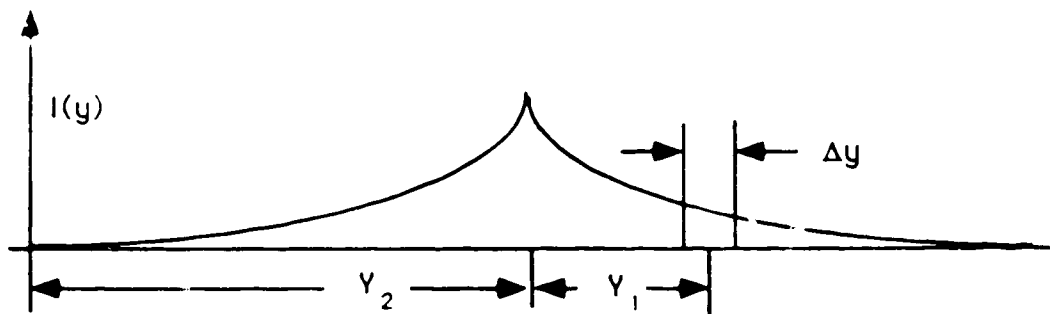


Figure 4-2. The strip of the intensity function which passes through the origin is shown. As the dose point, P is incrementally shifted towards the corner, the area $I(y_1)\Delta y$ is removed from the line integral of the strip.



However, if the point in question is incrementally shifted towards a corner, then a small section of the line integral will be removed, with each increment of the point, Δy , towards the corner, and an amount $l(y_1)\Delta y$ will be lost from the line integral, as shown in figure 4-2. The change in the dose gradient, $\frac{dD_p}{dx}$, caused by the increment Δy will then be:

$$\Delta \frac{dD_p}{dx} = l(y_1)\Delta y \quad \text{eqn. 4-3}$$

It is assumed that $l(y_1) \gg l(y_2)$, such that the contribution at y_2 is negligible. Taking the limit as $\Delta y \rightarrow 0$, we have a gradient expression for the source intensity, as a function of y_1 , the corner distance,

$$\frac{d}{dy} \left[\frac{dD_p}{dx} \right] = l(y_1) \quad \text{eqn. 4-4}$$

and if radial symmetry is assumed, then $r = y_1$ and,

$$\frac{d}{dy} \left[\frac{dD_p}{dx} \right] = l(r) \quad \text{eqn. 4-5}$$

Experimentally, dose profiles, $D(x)$, can be measured in air, along a number of segments perpendicular to the field edge and approaching a corner. These can be numerically differentiated with respect to x , in order to yield the dose gradients, $\frac{dD_p}{dx}$, at the field edge. These can in turn be differentiated with respect to y , and give the gradient of eqn. 4-5, which is equivalent to the extended source intensity function, $l(r)$. This was done for a $10 \times 10 \text{ cm}^2$ Co-60 field with an 80 cm source to probe distance, SPD.

The experimentally measured gradient labeled $I(r)$, is plotted vs the corner distance, r , in figure 4-3.

Figure 4-3 Plot of the measured gradient $d/dy[dD/dx]$, or the source intensity versus the corner distance, with the best fit exponential superimposed.

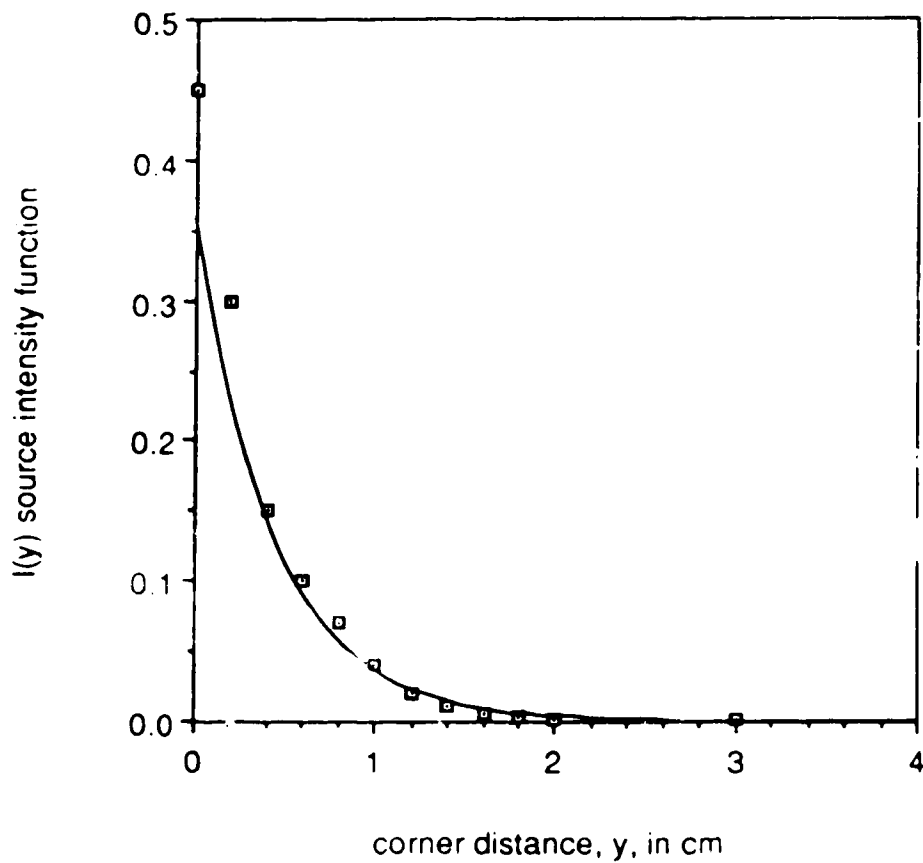
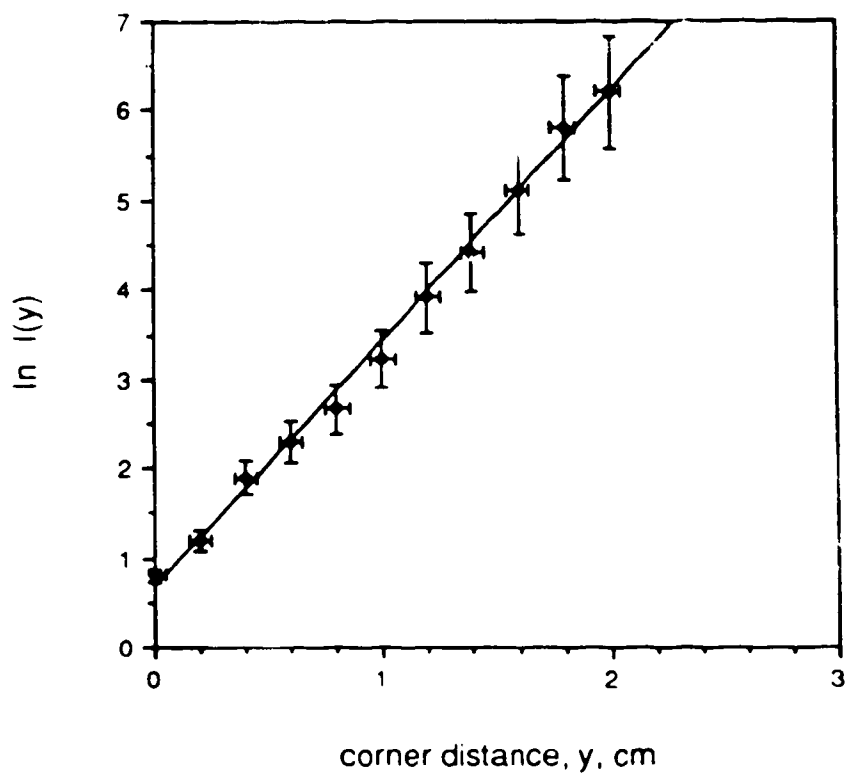


Figure 4-4 Plot of the natural log of the measured source intensity function versus the corner distance, with the best fit line superimposed



The log of the $I(r)$ data was then taken and plotted vs r so that the linear graph of figure 4-4 was obtained. Performing a least squares fit of the data allowed the parameters of the source function to be determined. The source function is of the form;

$$I(r) = C \exp\left[\frac{-\alpha}{sd} r\right] \quad \text{eqn. 4-6}$$

where C is a normalization constant, sd is the physical source diameter, and α is the parameter determined empirically.

The best fit line, with a correlation coefficient of 0.997, yields a value for α of 5.0, the minimum value within error is 4.1, and the maximum is 5.4. The error bars arise because a diode was used to perform the dose scans and since the measurements are near the field edge there is a large component of low energy scatter off the collimator which may create inaccuracies in the diode measurements, as discussed in section 3.4. The ion chamber could not be used for these measurements as it is too large to deliver the required spatial resolution. The minimum experimental value of α , 4.1 is only slightly larger than the value of 4.0 which was used for the Irreg+ calculations. In the Modified Irreg+ calculations for Co-60, the best fit value of 5.0 was used for α , the extended source parameter, and significant changes in the calculated effective transmission values resulted.

4.6 Discussion of the Results of the Modified Irreg+ Calculations.

As was mentioned, a new experimentally verified extended source parameter was used in the Modified Irreg+ program for the Co-60 calculations. Measured primary transmission estimates of the blocks were also used for the calculations in all three energies. The Modified Irreg+ calculations will now be commented on, and their accuracy compared to that of the original Irreg+.

4.6.1 Modified Irreg+ Results for Co-60

For Co-60 the Modified Irreg+ calculations showed some considerable improvement over Irreg+ in some cases, in others, however, either no improvement or a decrease in the accuracy occurred. Table 4-12 summarizes the rms errors between the measurements and both the Irreg+ and Modified Irreg+ calculations for all three block types.

table 4-12, Summary of rms errors for Co-60.

	SHIELD TYPE		
	2 x 7 cm ²	1 x 7 cm ²	Square
Irreg+ rms error	0.0148	0.0393	0.0690
Mod Irreg+ rms error	0.0188	0.0248	0.0387

Under the 2 x 7 cm² blocks, a small increase in the rms error is observed, the Modified Irreg+ program seemed to increase the number and

size of dose underpredictions in the data. With the narrower 1 x 7 cm² blocks the rms error is reduced significantly by the Modified Irreg+ calculations, and many of the severe dose overpredictions near the surface were reduced. However, some new significant errors were created in the 16 cm deep region. For the square occlusion shields also, an improvement in the rms error was observed and some of the largest errors were reduced, but again, new discrepancies were introduced with the Modified Irreg+ calculations.

In summary, the effect of using the larger extended source parameter of $\alpha = 5.0$, instead of $\alpha = 1.0$, is that the exponential intensity function increases more rapidly towards $r=0$, and the area under the curve is concentrated more towards the origin. This reduces the amount of source a point under a shielding block would 'see' in the source sector integration, and in general it causes a reduction in the effective transmission calculations. In some cases it has reduced the dose too much and created new significant errors which were not present in the original unaltered Irreg+ calculations.

4.62 Modified Irreg+ Results for 6 MV

Since the only change in the Modified Irreg+ calculations for 6 MV was the use of the measured narrow beam transmission estimates, the changes in the effective transmission results are small. The rms differences between the measurements and both calculations are given in table 4-13, no large changes occur.

table 4-13, Summary of rms errors for 6 MV.

	SHIELD TYPE		
	2 x 7 cm ²	1 x 7 cm ²	Square
Irreg+ rms error	0.0189	0.0198	0.0175
Mod Irreg+ rms error	0.0136	0.0192	0.0168

At 6 MV, small improvements are seen for the Modified Irreg+ calculations under all three block types. A few new significant errors were created under the rectangular blocks, but not under the square shields.

4.63 Modified Irreg+ Results for 15 MV

As with 6 MV, the only change in the Modified Irreg+ algorithm for 15 MV was the use of the measured narrow beam transmission estimates of the blocks. The rms differences are listed in table 4-14, and improvement occurs for all block types.

table 4-14, Summary of rms errors for 15 MV.

	SHIELD TYPE		
	2 x 7 cm ²	1 x 7 cm ²	Square
Irreg+ rms error	0.0200	0.0163	0.0187
Mod Irreg+ rms error	0.0182	0.0125	0.0177

In all the 15 MV Modified Irreg+ calculations, only two new significant errors were created and four were eliminated so an improvement in the results was gained by using the measured narrow beam transmission estimates.

CHAPTER 5

CONCLUSIONS

5.0 Summary and Conclusions

An extensive series of measurements along the central axis of closed to open field dose ratios under narrow shielding blocks for three photon energies have been compared to their calculated counterparts which were generated by the treatment planning program Irreg+. Overall, the Irreg+ algorithm performed well, by modelling the scatter and predicting the dose under the shielding blocks. In 82% of the cases tested, the difference between the calculated and measured doses was less than 3% of the open field dose. Of the discrepancies which were observed, most of them occurred under the thicker 'full' shielding blocks where the dose is reduced to such an extent that the discrepancies would not cause unacceptable doses to be delivered. The occurrences of the remaining discrepancies under the 'partial' shields were mostly under the 1 cm wide blocks and are partially correctable. The largest errors occurred in the Co-60 data, and were traced to an incorrect calculation of the amount of primary radiation which is 'seen' by the dose point. This was partially due to poor parameterization of the extended source model for Co-60, and incorrect values of the narrow beam transmissions of the blocks being entered into the program for all energies. The Irreg+ program was modified to correct for these deficiencies, however, while some of the significant discrepancies were reduced or eliminated, others were created by the Modified Irreg+ calculations.

It appears that the benefits of altering the extended source parameter in the Modified Irreg+ algorithm are not sufficient to warrant implementing these changes for clinical use. However, a small increase in the accuracy is

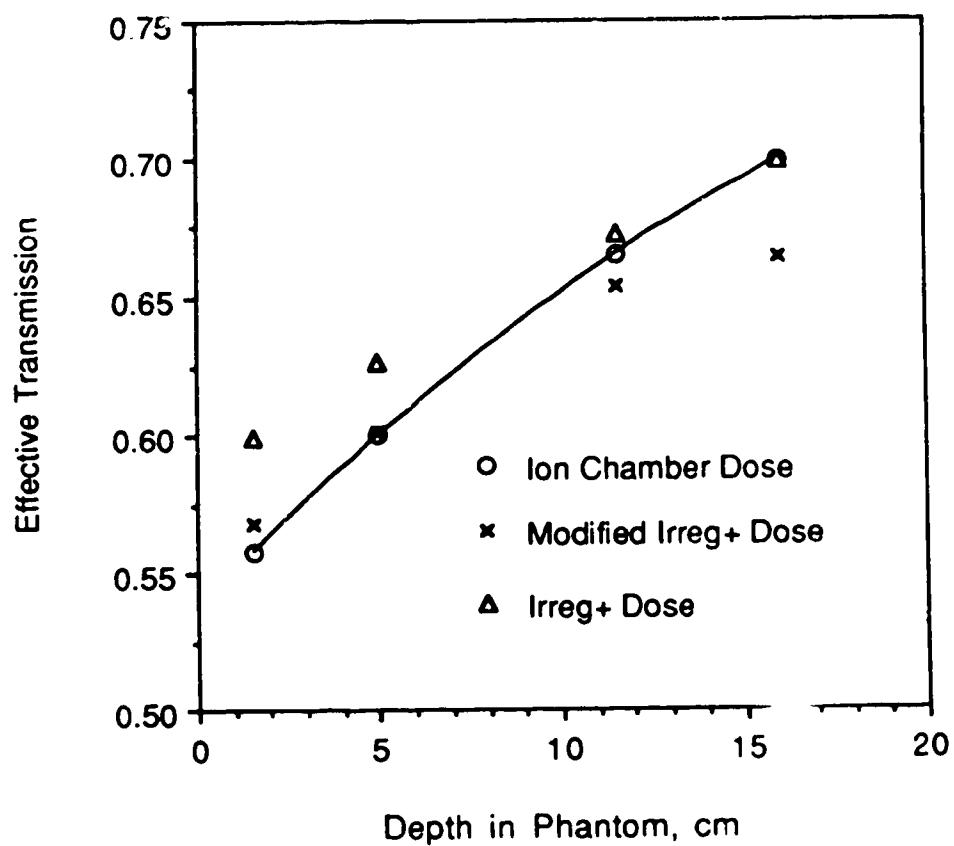
obtainable by making sure that the narrow beam transmission coefficients of the blocks, which are entered into the program, are correct. Clinically, it would be impractical to measure these each time a block is to be used, but a check of the physical thickness of a block could be made, to verify whether it is correct for the desired narrow beam attenuation. In conclusion, the Irreg+ program calculates the dose under narrow shielding blocks with reasonable accuracy, except for a few problem areas such as under the narrower blocks in Co-60. In these areas, an adjustment of the extended source parameter alone does not correct the algorithm; this only reduced and redistributed the significant discrepancies, rather than eliminating them.

5.1 Future Work

To continue this research, further investigation of the extended source model is necessary, for all three energies. Plotting the measured and calculated effective transmissions versus depth under a 1 x 7 cm², 5 HVT thick shield in a 10 x 10 cm² Co-60 field, as is shown in figure 5-1, hints at a possible direction this investigation should take.

It is observed on the graph that the curvature of the calculated data is different from that of the measured data. Also, altering the extended source parameter, α , for the Modified Irreg+ calculations changed the offset of the calculated data, but had only a slight effect on its curvature. Another observation is that a value of $\alpha = 5$ gives good results close to the surface, and, $\alpha = 4$ gives good results deeper in the phantom. From this it appears that to obtain better agreement between the measurements and the calculations that the extended source parameter α may have to be made a function of depth, or source distance, and possibly field size.

Figure 5-1 Measured and calculated effective transmissions vs depth under a $1 \times 7 \text{ cm}^2$, 1 HVT shielding block in a $25 \times 25 \text{ cm}^2$ Co-60 field.



A complete investigation is necessary which includes measuring the source parameter α , as described in section 4.6, for many different source distances and field sizes, to determine whether a dependence on these parameters exists. As changing the field size and the source distance alter the scatter conditions of the set up, it would not be unlikely for the extended source intensity distribution function to show a dependence on these variables.

REFERENCES

6.0 References

1. Buschke, Parker, R.G., Radiation Therapy in Cancer Management, Grune and Stratton, New York, 1972.
2. IRCU Report, #24, Determination of Absorbed Dose in a Patient Irradiated by Beams of X or Gamma Rays in Radiotherapy Procedures., International Commission on Radiation Units and Measurement., Washington D.C., 1976.
3. Cunningham, J.R., Shrivastava, P.N., Wilkinson, J.M., Program Irreg - Calculation of Dose from Irregularly Shaped Photon Beams., Computer Programs in Biomedicine 2 (1972) 192-199, North-Holland Publishing Company
4. Clarkson, J.R., A note on depth doses in fields of irregular shape. Br J Radiol 14:265, 1941
5. Tatcher, M., A Comparison of Commercial Treatment Planning Systems When Calculating Dose Under Shielding Blocks., I.J . Radiation Oncology. Biology. Physics. Vol.12, Num.10., Oct. 1986.
6. Johns, H.E., Cunningham, J.R., The Physics of Radiology, 4th edition. Springfield Illinios, Thomas..1983.
7. Hubbe. J.H., NSRDS-NBS #29, Washington, D.C., 1969.
8. Evans, R.D., The Atomic Nucleus, New York, McGraw-Hill Book Company, c.1955.
9. Patterson, W.H., and Thomas, R.H., Accelerator Health Physics, Accademic Press, New York, 1973.

10. IRCU Report, #23, Measurement of Absorbed Dose in a Phantom Irradiated by a Single Beam of X or Gamma Rays. International Commission on Radiation Units and Measurement., Washington D.C., 1973.
11. Wilkinson, J. M., Rawlinson, J. A., Cunningham, J.R., An Extended Source Model for the Calculation of the Primary Component of a Cobalt-60 Radiation Beam in Penumbra Regions, Presented at the A.A.P.M. meeting, Washington, July 14, 1970.
12. Suzuki, A., Suzuki, M.N., Capintec Ionization Chamber Probes for Exposure Measurement, Capintec Incorporated, Montvale, New Jersey.
13. Mota, H.C., Vijaykumar, S., Sibata, C., Higgins, P., Thomas, F., Saxton, J., Weinstein, M., Posterior Spinal Cord Block: A Dosimetric Study, Presented at 73rd Annual Meeting of RSNA (1987), submitted to Radiology, Nov. 87.
14. Rikner, G., Patient dose measurements in photon fields by means of silicon semiconductor detectors. Medical Physics, Vol 14, No. 5, Sept/Oct 1987.

